# ENHANCED FEM-DBEM APPROACH FOR FATIGUE CRACK-GROWTH SIMULATION

**Venanzio Giannella**

*Unione Europea*


UNIVERSITÀ DEGLI
STUDI DI SALERNO

**FONDO SOCIALE EUROPEO**

**Programma Operativo Nazionale 2000/2006**
**"Ricerca Scientifica, Sviluppo Tecnologico, Alta Formazione"**
**Regioni dell'Obiettivo 1 – Misura III.4**
**"Formazione superiore ed universitaria"**

***Department of Industrial Engineering***

*Ph.D. Course in Mechanical Engineering*
*(XVI Cycle-New Series, XXX Cycle)*

# ENHANCED FEM-DBEM APPROACH FOR FATIGUE CRACK-GROWTH SIMULATION

**Supervisor**
*Prof. Roberto Guglielmo Citarella*

**Ph.D. student**
*Venanzio Giannella*

**Scientific Referee**
*Prof. Renato Esposito*

**Ph.D. Course Coordinator**
*Prof. Ernesto Reverchon*

# List of publications

R. Citarella, V. Giannella, M. Lepore, DBEM crack propagation for nonlinear fracture problems, Frattura ed Integrità Strutturale, 34 (2015) 514-523; DOI: 10.3221/IGF-ESIS.34.57.

R. Citarella, V. Giannella, E. Vivo, M. Mazzeo, FEM-DBEM approach for crack propagation in a low pressure aeroengine turbine vane segment, Theoretical and Applied Fracture Mechanics, Volume 86, Part B, December 2016, Pages 143-152, DOI: 10.1016/j.tafmec.2016.05.004.

R. Citarella, V. Giannella, M. Lepore, G. Dhondt, Dual boundary element method and finite element method for mixed-mode crack propagation simulations in a cracked hollow shaft, DOI: 10.1111/ffe.12655.

V. Giannella, J. Fellinger, M. Perrella, R. Citarella, Fatigue life assessment in lateral support element of a magnet for nuclear fusion experiment "Wendelstein 7-X", Engineering Fracture Mechanics, Volume 178, 1 June 2017, Pages 243-257, DOI: 10.1016/j.engfracmech.2017.04.033.

R.C. Wolf, V. Giannella, et alii., Major results from the first plasma campaign of the Wendelstein 7-X stellarator, DOI: 10.1088/1741-4326/aa770d.

V. Giannella, M. Perrella, R. Citarella, Efficient FEM-DBEM coupled approach for crack propagation simulations, Theoretical and Applied Fracture Mechanics, Volume 91, October 2017, Pages 76-85, DOI: 10.1016/j.tafmec.2017.04.003.

R. Citarella, V. Giannella, M. Lepore, J. Fellinger, FEM-DBEM approach to analyse crack scenarios in a baffle cooling pipe undergoing heat flux from the plasma, 2017, AIMS Journal 4(2):391-412, 2017, DOI: 10.3934/matersci.2017.2.391.

V. Giannella, R. Citarella, J. Fellinger, R. Esposito, LCF assessment on heat shield components of nuclear fusion experiment “Wendelstein 7-X” by critical plane criteria, Procedia Structural Integrity 8 (2018) 318-331.

# Summary

# List of figures

# List of tables

# Abstract

To comply with fatigue life requirements, it is often necessary to carry out fracture mechanics assessments of structural components undergoing cyclic loadings. Fatigue growth analysis of cracks is one of the most important aspects of the structural integrity prediction for components (bars, wires, bolts, shafts, etc.) in presence of initial or accumulated in- service damage. Stresses and strains due to mechanical as well as thermal, electromagnetical, etc., loading conditions are typical for the components of engineering structures. The problem of residual fatigue life prediction of such type of structural elements is complex, and a closed form solution is usually not available because the applied loads not rarely lead to mixed-mode conditions.

Frequently, engineering structures are modelled by using the Finite Element Method (FEM) due to the availability of many well- known commercial packages, a widespread use of the method and its well-known flexibility when dealing with complex structures. However, modelling crack-growth with FEM involves complex remeshing processes as the crack propagates, especially when mixed- mode conditions occur. Hence, extended FEMs (XFEMs) and meshless methods have been widely and successfully applied to crack propagation analyses in the last years. These techniques allow a mesh- independent crack representation, and remeshing is not even required to model the crack growth. The drawbacks of such mesh independency consist of high complexity of the finite elements, of material law formulation and solver algorithm.

On the other hand, the Dual Boundary Element Method (DBEM) both simplifies the meshing processes and accurately characterizes the singular stress fields at the crack tips (linear assumption must be verified). Furthermore, it can be easily used in combination with FEM and, such a combination between DBEM and FEM, allows to simulate fracture problems leveraging on the high accuracy of DBEM when working on fracture, and on the versatility of FEM when working on complex structural problems.

Generally, FEM is used to tackle the global complex structural problem, assessing the fields of displacements, strains and stresses; subsequently, such fields are used to obtain the boundary conditions to apply on a DBEM submodel that bounds the region in which the crack is present. In this way, the

fracture problem is solved in the DBEM environment allowing to take advantage of its inherently simpler remeshing process. Such FEM-DBEM "classical" approach has been previously implemented under fixed either displacements or tractions boundary conditions applied on the DBEM submodel cut surfaces, without updating of their values during the propagation. Such boundary conditions are consequently assumed to be insensitive to the submodel stiffness variation due to the crack-growth, with the consequent introduction of an element of approximation that limits the accuracy of results. In case of traction boundary conditions the approach provides conservative results in terms of residual life cycles, whereas, non-conservative results are obtained in case of fixed displacements boundary conditions. Interestingly, the here proposed alternative approach provides results comprised between the upper and lower bounds given by such two classical approaches.

This work presents an enhanced FEM-DBEM submodelling approach to simulate fracture problems through the adoption of the principle of linear superposition. Theoretical background can be found in the literature, where the J-integral for a thermal-stress crack problem was retrieved by a simple application of a load distribution on the crack faces (as provided by the uncracked problem solution) instead of the application of the inherent displacement or traction condition on the model boundary. This idea has been here widely extended to more complex analyses allowing to solve fracture problems with very high accuracy by means of relatively simple DBEM stress analyses, even when the global analyses present thermal loads, contacts, friction, electromagnetic fields, etc. As a matter of fact, all the complexities are tackled by a global FEM analysis on the uncracked domain, whereas, the objectives of correctly predicting the whole crack-growth are completely demanded to the DBEM.

The methodology has been validated comparing the results with those provided by different numerical approaches, like the well-established classical FEM-DBEM approaches or fully FEM based approaches, as available from literature.

Then, some industrial applications have been analysed by means of this new methodology showing that the procedure can also handle problems of higher complexity leading to an accuracy on the results that, in some cases, could not even be obtained with the classical approaches.

# Introduction

## *I General aspects*

Starting from the industrial revolution around the late 18th century, metals were seen as the most successful and all-purpose construction materials. They were mainly chosen for their high strength to weight ratio, workability and availability. Today many buildings, ships, aircrafts and many other engineering structures are still largely built out of metals. Unfortunately, many of this metal structures did not live as per their expectations and many of them collapsed catastrophically under regular service conditions. Furthermore, most of these structural failures occurred very often without adequate warnings and, as a result, many human lives have been lost. The cause of such catastrophic failures (Figs. 1-2) could often be attributed to a combination of material deficiencies in the form of pre-existing flaws in the material, poor designs, in-service damages, etc.

To ensure safety, current specific standards require routine periodic checks for detecting possible cracks. Then, cracked components have to be monitored and, if necessary, replaced or repaired before they become critical. Improvement at the design stage, where high stress concentrations in the structure should be avoided, better production methods as well as enhancement of material properties have all helped to minimize the criticalities and consequently have reduced the number of failures. However, total elimination of cracks is not only impractical but also impossible because cracks often develop well below the material yield strength. To further mitigate fracture failures, the so called design philosophy "*Damage Tolerance*" has been introduced in recent years at the design stage where engineers have to anticipate the likelihood of cracks in the structural components.

As structures are becoming more complex, the need for an accurate and reliable assessment of the structural safety has become mandatory. A simple arbitrary safety factor is no longer an acceptable safety margin, nor is it justified in terms of economy and efficiency. The need for reliable engineering decisions has prompted the development of a methodology to compensate for the inadequacies of conventional design concepts. Although the conventional

design criteria based on the material strength can be adequate for many engineering structures, they are insufficient when there is the likelihood of native and/or accumulated in-service defects.

In this framework, Fracture Mechanics is often used to provide the necessary additional safety checks, understandings of the fracture processes and, even more important, obtaining reliable predictions on the residual strength of the structure.

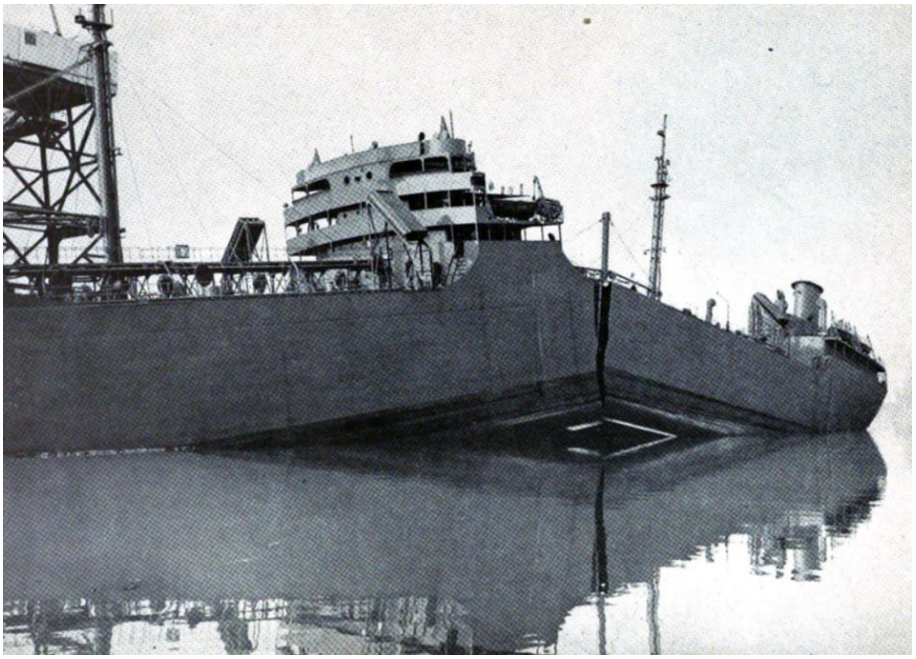

**Figure 1** *Example of brittle fracture of a Liberty ship after splitting in two at her outfitting dock; welded structure, rather than bolted, offered a continuous path to cracks to propagate throughout the entire structure (Parker, 1957)*

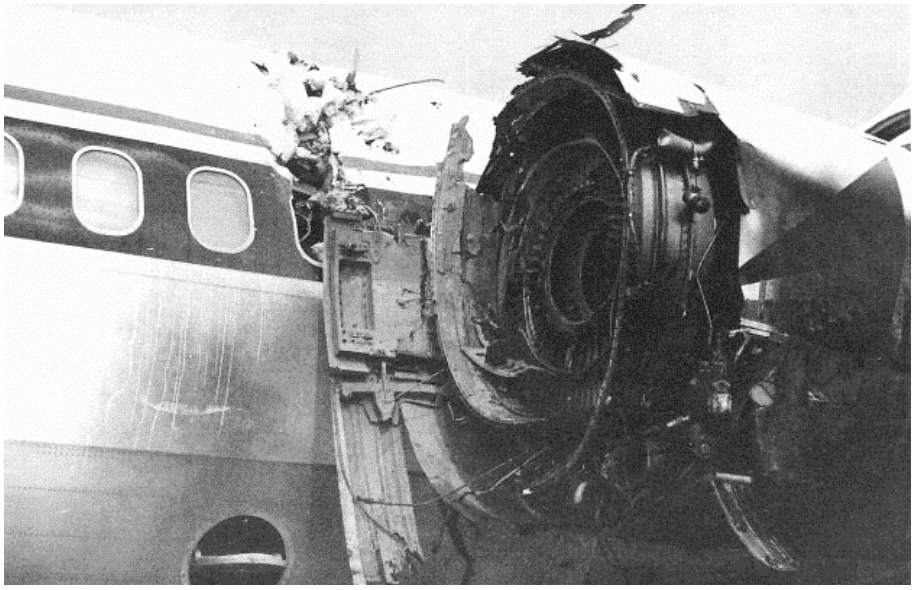

***Figure 2*** *Example of fatigue crack-growth in a turbofan engine (Pratt & Whitney JT8D) occurred during the take-off roll; a fan disk penetrated the left aft fuselage determining two fatalities (www.wikipedia.it).*

## *II Fracture Mechanics*

Beginning with catastrophic failures of railway components through to serious failures of many Liberty ships during World War II, there are many grim examples of the debilitating effects of flaws on the material strength. It has also emerged during this century that the conventional criteria of tensile strength, yield strength and buckling stress are not always sufficient to guarantee the overall component integrity. This has been especially evident with the introduction of high strength materials, which are correspondingly low in crack resistance. Furthermore, structural engineers are continuously struggling to reduce safety margins between the stresses expected during the working conditions and the strength of materials. All of these conditions have spurred the development of Fracture Mechanics, especially in the last two decades, to enable dedicated analyses of components with crack-like defects.

The discipline of Fracture Mechanics (Anderson, 1991) enables the prediction of crack behaviour to be quantitatively achieved. Namely, Fracture Mechanics has been used to predict the crack size below which no crack-growth would occur, or, the crack size at which a component would fail given a certain applied fatigue load. In between these two limits, Fracture Mechanics allows to estimate the rate of crack-growth and then allows to predict the life of a cracked component under fatigue loading. This allowed going beyond the

traditional design standpoint (Fig. 3a), in which only the requested loads were compared with the material strength, to the concept of *Damage Tolerance* design process (Fig. 3b), in which also the presence of defects has to be taken into account in the process. Fracture Mechanics analyses are then carried out to obtain the component life with a pre-defined initial flaw size and the expected fatigue loading conditions. Such life must exceed the operational life needed for a given structure otherwise the component geometry has to be redesigned or, otherwise, the loading revised. Inspection intervals can then be set to ensure that crack-growth is less than that predicted or, if not, the component has to be either repaired or replaced.

Fracture Mechanics is based on continuum mechanics concepts, which express given relationships between the stress and displacement fields at the crack tips. Under the small strains and linear elastic assumptions, it is found that the stress fields in close vicinity of the crack tip are inversely proportional to the square root of the distance from the tip itself. The constant of proportionality is the Stress Intensity Factor (SIF), which defines the intensity of the singular stress field at the crack tip. It is also found from experiments that failure occurs when, under static load conditions, the SIF reaches the critical value for the material and, therefore, an accurate determination of SIF is of extreme importance for the consequent estimate of the structural integrity. Moreover, when dealing with fatigue loading conditions, the precise SIF evaluation is of utmost importance for the Crack-Growth Rate (CGR) prediction and eventually for the residual fatigue life assessment.

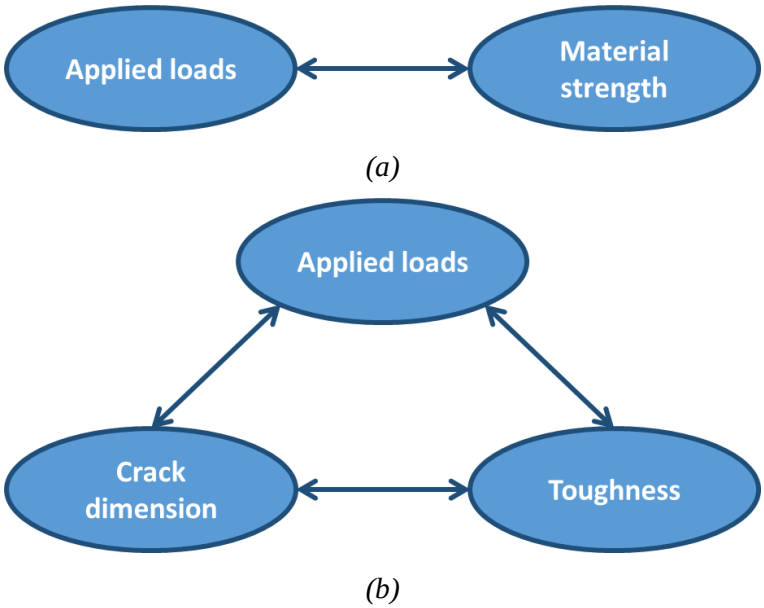


***Figure 3*** *(a) Traditional designing philosophy vs. (b) Damage Tolerance designing philosophy.*

## *III Numerical analyses*

Obviously, analytical techniques cannot tackle all the complexities encountered in all the engineering structural components. Therefore, numerical techniques have been widely developed in recent years, encouraged especially by the enormous advances in the computer technology.

Nowadays, FEM is the most widely used in the engineering designing process thanks to its advantages when simulating several physical phenomena. The method is widely used in the industries since it is able to face problems involving: contacts, frictions, mechanical, thermal and electromagnetical loads, complex constitutive law formulations, impacts, etc. There are various ways of tackling Fracture Mechanics by FEM and, definitely, FEM has been efficiently used along the years in several applications. However, it typically needs long model preparation times. In addition, especially when the crack propagates generating complex three-dimensional shapes, the method is not anymore suitable to simulate the fracture process due to distortion of elements nearby the crack, too long runtimes, etc.

The Boundary Element Method, together with its enhanced version Dual BEM, can circumvent the limitations of FEM on complex crack propagation problems (Aliabadi, 1991, 1992; Brebbia, 1984, 1989). This method is based on the solution of integral equations, that govern elasticity and potential theory. Such a method works with the discretization of the only boundary into elements over which the product of shape functions, Green's functions and element Jacobians, are numerically integrated. This results in higher accuracy particularly when the domain to be discretised contains regions of high stress gradients (such as cracks) which would necessitate a considerable concentration of FEM elements and nodes. Hence, DBEM is particularly suited to Fracture Mechanics analyses due to the accuracy of the results and the inherently better and simpler remeshing process as the crack increases in size.

Since only the boundaries of the domain are discretised, the dimensionality of the domain is reduced by one, reducing then the size of the mathematical problem to handle (Fig. 4). However, the system matrix is unsymmetric and fully populated and therefore, generally, it takes longer runtimes than those needed by FEM to obtain the solution. More generally, considering the computational power nowadays available, DBEM remains more attractive, when working on fracture, comparing the preprocessing efforts of the two aforesaid numerical methods (Fig. 5).

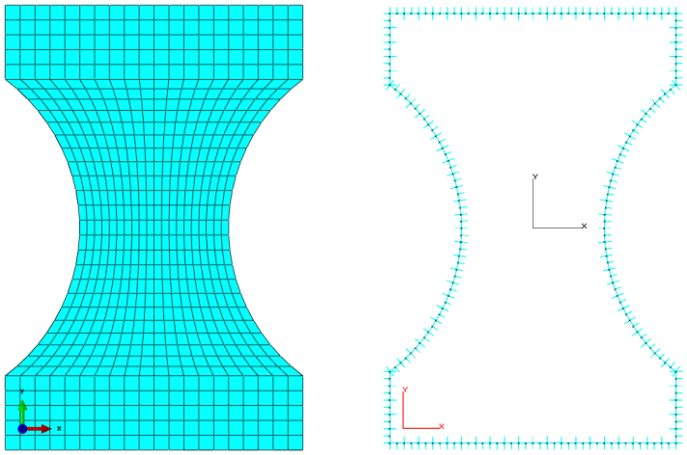

*(a)* *(b)*

***Figure 4*** *Example of a 2D model via (a) FEM and (b) BEM.*

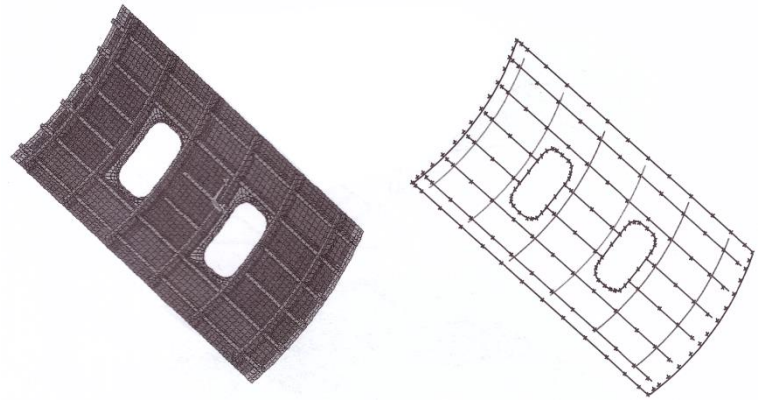

*(a)* *(b)*

***Figure 5*** *Example of (a) FEM and (b) BEM models of a reinforced curved fuselage panel (Aliabadi, 2002)*

## *IV Boundary Element Method (BEM) and Dual BEM*

BEM has become established as an effective alternative to FEM in several important areas of engineering analysis. Although the BEM, also known as the Boundary Integral Equation (BIE) method, is a relatively new technique for engineering analysis the fundamentals can be traced back to classical mathematical formulations by Fredholm (Fredholm, 1903) and Mikhlin (Mikhlin, 1957) in potential theory and Betti (Betti, 1872), Somigliana (Somigliana, 1886) and Kupradze (Kupradze, 1965) in elasticity.

Basically, the aim is to transform the governing differential equations defined in the domain into an integral equation which applies only to the boundary of the domain. Such an integral equation depends on the availability of:

- a fundamental solution to the governing differential equation for a point force;
- a reciprocal relationship (such as Green's theorem; Green, 1828) between two functions which are continuous and possess continuous first derivatives.

The choice of the unknowns has led to two formulations of the boundary integral equations: the direct method, where the unknowns are the actual physical variables in the problem, such as displacement or traction in elasticity; the indirect method that historically precedes the previous one. In the latter approach, the unknowns are fictitious density functions which have no physical significance but from which the physical unknowns can be obtained by postprocess.

In order to obtain the boundary integral equations, a powerful and general technique is the weighted residual method of Brebbia (1977, 1978) where the error residual is minimized. Jeng and Wexler used a variational formulation similar to that of the finite elements and Cruse and Rizzo (Rizzo, 1967; Cruse, 1969) employed Betti's reciprocal work theorem.

For many years, the potential of boundary integral equations was not realized due to the difficulty of attaining analytical solutions to the integral equations for practical problems and due its essentially mathematical origins. However, research into the numerical solution of boundary integral equations was prompted by the advent of high speed computing. As computers grew in power and storage, the amenable problems became more complex. This resulted in the numerical method now known as BEM. Brebbia demonstrated that not only it is related to FEM but that both methods can be derived from the same variational equation (Brebbia, 1978).

In the BEM, the boundary integral equations are discretized so that numerical integration is carried out over a small part (element) of the boundary, over which the variation of the boundary variables is expected to be small. Variation over an element is handled in a similar way to that of the finite elements. For example, considering an elastostatic problem, the variation of displacements and tractions over an element is approximated by opportune shape functions related to nodal values of displacements and tractions respectively. Each collocation node will yield either two or three boundary integral equations depending on the dimensionality of the problem. By moving this collocation point to each node in the model, a system of equations is built up in which the displacement at each point is related to the displacement and tractions on all points on the boundary. The resulting matrices are therefore fully populated and unsymmetric. This is in contrast to

the sparse and banded FEM system matrix which, however, are generally much larger for an equivalent problem.

It is worth noting that only the boundary of the model needs to be discretized as the governing (elastostatic) differential equations are satisfied in the interior region. The data preparation is carried out only for the boundary, avoiding the domain discretization used by the FEM. This results in a method that is particularly suited to Fracture Mechanics analyses due to the accuracy of the results both on the surface and at selected interior points.

The introduction of isoparametric variation over the boundary elements by Lachat and Lachat & Watson (Lachat, 1975, 1976) provided a further possibility to the BEM to fulfil its potential of high accuracy and efficiency. Quadratic variation of geometry was used over the elements and linear, isoparametric quadratic and cubic variation of the unknown displacement and traction were catered for. This enables the BEM to be more economical than FEM for certain types of problems, although FEM will be more appropriate for others. Anyway, both techniques should be made available to engineers.
The adopted DBEM approach (Portela, 1990, 1993; Apicella, 1994; Mi, 1994; Fedelinsky, 1994) is a BEM enriched with special discontinuous elements appropriate to consider nodes and faces of the crack topologically coincident. The three-dimensional domain boundary is discretized into either 4, 8 or 9 noded quadrilateral elements, or 3 or 6 noded triangular elements. The boundary integral equations here adopted apply to a homogeneous isotropic domain and the linear elastic assumption must also be held. As aforesaid, with DBEM, only the crack faces and the other boundaries are discretized. Traction boundary integral equations are used for one crack face and displacement boundary integral equations are used for the second crack face and the remaining boundaries. So doing, being the traction and displacement equations independent, the system coefficient matrix turns out to be non-singular and, therefore, the solution can be retrieved.

## *V Description of Thesis*

After an introduction, in chapter I it has been discussed on how to couple the FEM and DBEM methods to work out general Fracture Mechanics problems. At first, the need to adopt a submodelling strategy when solving fracture problems on large structures has been introduced. Then, it has been argued on how to implement such a submodelling technique by using the FEM and DBEM methods. Three FEM-DBEM submodelling approaches have been presented and the advantages of using the “Loaded Crack” (LC) approach highlighted. By means of such an approach, based on loading only the DBEM crack faces, the most accurate results in terms of SIFs, CGRs and crack paths can be obtained.

In chapter II, it has been shown how the LC approach has been applied on a shaft-hub coupling that undergoes different loading conditions. The results have been compared with those obtained by leveraging on a pure DBEM approach and with two different FEM codes showing a very sound agreement.

A first industrial application of the LC approach has been presented in chapter III. It consisted in a crack propagation simulation in an airfoil of a statoric segment of a GE-Aviation aeroengine. The LC approach turned out to be more efficient in terms of computational effort and more accurate in terms of fatigue life estimate, when compared with a classical FEM-DBEM approach.

In chapter IV, it has been presented a further industrial application of the three FEM-DBEM approaches on a component of the magnetic cage of the nuclear fusion experiment "Wendelstein 7-X". The residual fatigue life has been estimated with all the approaches and the results compared and discussed. Again, the LC approach turned out to be more accurate than the classical approaches.

All the DBEM and FEM-DBEM calculations shown in chapters II-IV were executed on a workstation with the following general configuration: motherboard MSI X99S SLI Plus, CPU Intel i7-5820K with 15MB L3 cache, RAM 8x 8GB HyperX Fury DDR4, SSD Samsung 850 2x 250GB and Windows 7 Professional 64bit SP1.

At the end, final conclusions have been summarised.

# Chapter I
# FEM-DBEM approaches to Fracture Mechanics

## *I.1 Introduction*

FEM and BEM are effective tools for the numerical analysis of many physical problems described with a set of partial differential equations and frequently impossible to solve analytically.

With regard to particular aspects, the two methodologies are complementary, each of them having preferential applications. Namely, FEM is well suited for complex analyses containing nonlinearities, massive meshes, contacts, anisotropic materials, etc., whereas BEM and in particular DBEM (Dual BEM) (Aliabadi, 1992a, 1992b; Portela, 1990; Fedelinsky, 1994) are generally preferred in the Linear Elastic Fracture Mechanics (LEFM) context, to get accurate SIFs (Stress Intensity Factors) evaluations and automatic crack propagations (Apicella, 1994).

Although the fracture phenomenon plays essentially a local effect if compared to the overall structure (i.e. the singular fields at crack tip, the possible crack propagation, etc.), it cannot be overlooked. An initial small crack, after it propagates throughout the structure, can lead to the failure of the entire structure as taught by well-known past catastrophic failures (Figs. I.1, I.2). Numerical analysis can be used as a tool to better understand how fracture phenomena affect structures in order to prevent catastrophic failures.

When one or more cracks have to be numerically modelled in large structures, a submodelling approach is generally mandatory in order to make the approach amenable from a computational standpoint and also to reduce the size of the models to handle. Especially when such structures are modelled by FEM, this submodelling approach plays an even more important role since the cracks would need very fine meshes in their surroundings with the consequent sharp increase of runtimes. The DBEM would be more attractive in this context thanks to its intrinsic nature of meshing only the model boundaries and one or multiple cracks can be modelled more easily than by

FEM. However, the inherent restrictions of the DBEM do not allow tackling all the industrial problems as a standalone tool.

As a consequence, great research efforts have been aimed along the years at improving the synergetic usage of the two previously mentioned methodologies (McNamee), in order to exploit the FEM versatility in combination with the intrinsic better features of DBEM for modelling fracture. This work presents three approaches that allow to adopt a submodelling approach (Fig. I.1), to strongly reduce the runtimes, and specifically a FEM-DBEM coupling, to get the highest accuracy on results by benefiting from both the diverse advantages of FEM and DBEM.

Two approaches are based on replicating the FEM global fields in a DBEM local submodel, where the fracture problem is worked out. These two approaches provide an upper and a lower bound in terms of residual fatigue life estimate. We will see how, the third approach, based on the application of the superposition principle to Fracture Mechanics problems, provides the most efficient and accurate fracture assessment.

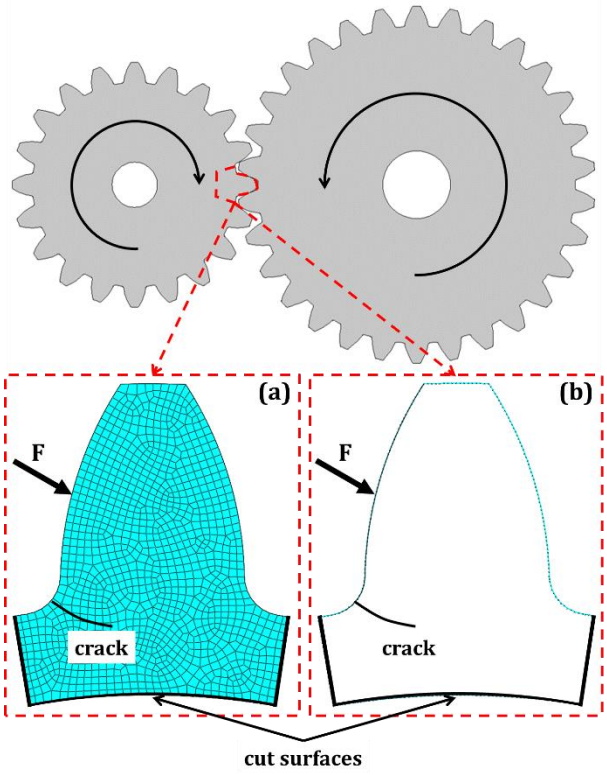


***Figure I. 1*** *Example of a (a) FEM and a (b) DBEM submodelling of a gear tooth with a crack (2D problem).*

## *I.2 Superposition principle for Linear Elastic Fracture Mechanics*

Wilson (Wilson, 1979) showed that the SIFs for a crack in a 2D thermal-stress problem could be calculated by means of a simpler stress analysis in which no external loads were applied but just tractions on the crack faces. This was possible leveraging on the principle of linear superposition applied to a Fracture Mechanics problem, as explained in the followings.

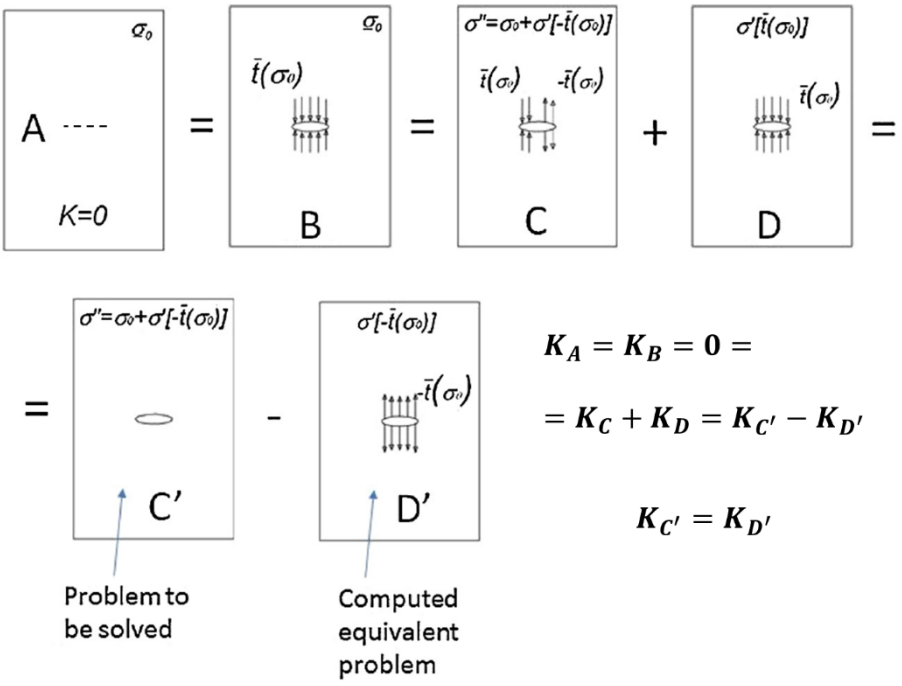


***Figure I. 2*** *Superposition principle applied to a fracture problem; $\underline{\sigma}_0$ is the pre-existing stress field generated by the applied prescribed conditions, etc.*

Extending the Wilson's example to the most general crack problem schematically shown in Fig. I.2, the superposition principle can be then applied as explained in the following steps:

- from an original uncracked domain (A), a crack can be opened (B) and loaded with tractions equal to those calculated over the same dashed line in (A);
- the new configuration (B), perfectly equivalent to (A), can then be transformed by using the superposition principle, splitting the boundary conditions as in (C) and (D);
- (C = C') represents the real fracture problem to be solved, whereas (D), after the tractions sign inversion, turns in an equivalent problem (D') that will be effectively tackled.

In conclusion, using boundary conditions retrieved from the considered uncracked problem (A), a purely stress crack problem (D') can be considered for the fracture assessment; in such equivalent problem, the crack faces undergo tractions equal in magnitude but opposite in sign to those calculated over the same (dashed) crack line in (A). In other words, SIFs for case (C') are equal to those calculated for the simpler problem (D'). In final, the use of the superposition principle enables a faster convergence for the simpler DBEM pure stress analyses, in comparison with that provided by the more traditional FEM-DBEM approaches (those with transfer of displacement or traction boundary conditions on the submodel cut surfaces), with consequent reduction of computational burden.

## *I.3 FEM-DBEM coupled approaches*

Considering the different FEM and DBEM capabilities, the most promising idea would be to use FEM to calculate the global displacement-strain-stress fields and to adopt such results to solve the local fracture problem by means of DBEM.

Here, two FEM-DBEM approaches are presented and, by considering the superposition principle explained in §I.2, a third one is proposed. The three approaches can be schematically explained by means of Fig. I.3. With reference to cases *(b)* and *(c)* in Fig. I.3, all the rigid body degrees of freedom have to be eliminated and this can done, as instance, by applying springs of negligible stiffness on few elements.

Basically, all the approaches are based on the submodelling technique in order to strongly reduce the computational efforts. The basic assumption is that the analysed fracture phenomena do not introduce a significant perturbation on the overall fields far from the crack area, so that, there is no need to explicitly model the entire structure for the fracture assessment.

A DBEM submodel can be then extracted by a Boolean operation of subtraction between the FEM model and a user defined cutting domain, providing, in the DBEM environment, a smaller model that surrounds the crack insertion area with just a surface mesh at its boundaries.

After the DBEM submodel extraction, a crack is inserted in the submodel and a remeshing, which typically involves just the crack surroundings, is realised. Subsequently, such DBEM cracked submodel is loaded with apposite boundary conditions in order to compute SIFs representative of those occurring in the real cracked component. Then, when requested, the crack propagation can be simulated by increasing step-by-step the crack dimensions, with the $i^{th}$ crack kinking and growth rate evaluated as a function of the SIFs evaluated for the $(i\text{-}1)^{th}$ geometry. Moreover, for fatigue crack propagation simulations, one or more load cases are used to assemble the needed fatigue load spectra representative of the loads occurring during the real operation of

the components. Also, it has to be guaranteed that the crack tips remain adequately far from the cut surface boundaries over which displacements or traction were imposed.

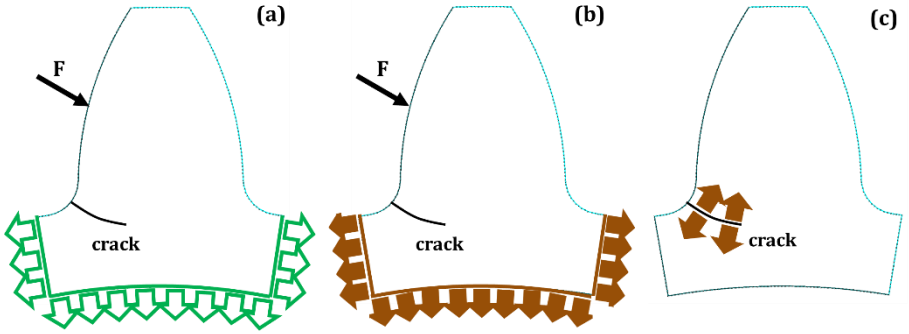


***Figure I. 3*** *Different approaches for the selection of the DBEM submodel loading conditions for a gear tooth with a crack: (a) Fixed Displacement (FD); (b) Fixed Load (FL); (c) Loaded Crack (LC).*

The DBEM submodel loading process can follow one of the three different previously mentioned approaches (example in Fig. I.3) explained in the following:

- Fixed Displacement (FD) approach: the DBEM volume cut surfaces are loaded with displacement boundary conditions;
- Fixed Load (FL) approach: the DBEM volume cut surfaces are loaded with traction boundary conditions;
- Loaded Crack (LC) approach: the DBEM crack faces are loaded with traction boundary conditions.

In detail, two kind of inaccuracies unavoidably arise when using both FD or FL approaches. Firstly, such two approaches use boundary conditions that applied to a cracked model come from an uncracked global model. Secondly, boundary conditions are kept as fixed during the crack propagation simulation and therefore they are considered as insensitive to the continuously decreasing DBEM submodel stiffness induced by the growing crack. Both inaccuracies could be overcome by using a larger submodel but this would affect the runtimes without even completely eliminate such drawbacks. Anyway, the FD approach has been satisfactorily implemented in the past as in some works available in the literature (Citarella, 2013, 2014).

On the contrary, the LC approach allows to inherently consider step-by-step updated boundary conditions, since additional loading is provided on the crack extension area at each step of the incremental crack-growth simulation. In addition, the SIFs are rigorously calculated even by using boundary conditions that are coming from an uncracked model, as dictated by the superposition principle (§I.2). Moreover, there is no need to replicate the global FEM fields in the DBEM submodel and this widen the range of

amenable applications, namely more complex analyses can be restricted solely to FEM approach.

For these reasons, in the following it is shown that the LC approach represents the most enhanced strategy to couple FEM and DBEM, providing results with the highest accuracy in terms of SIF assessment and therefore also in terms of residual fatigue life estimate and crack path assessment. Such an approach is proposed in the current work by means of a FEM-DBEM submodelling strategy but, however, it can clearly be also applicable to FEM-FEM submodelling strategies or equivalents. It is worth noting that, for embedded cracks far enough from the external boundaries (e.g. voids, internal cracks), it would be possible to consider the cracks as in an infinite body so the DBEM boundary would be just the loaded crack faces and the corresponding mathematical problem notably reduced.

Besides the submodel loading conditions, in order to predict a Linear Elastic Fracture Mechanics (LEFM) incremental crack-growth, three basic criteria are required for the separate phases of: SIF evaluation, kink angle prediction and Crack-Growth Rate (CGR) assessment. The criteria that have been used in the current work are described in the followings together with some references about the most widely accepted ones.

## *I.4 Crack-growth criteria*

A crack-growth simulation is typically worked out by means of an incremental crack-extension analysis in which the three distinct phases of SIF evaluation, kink angle prediction and CGR assessment are basically repeated until either a requested crack size or a critical K value is reached. Namely, for each crack extension, the SIFs are calculated and used to predict both the direction of the growth and the corresponding fatigue cycles. Various criteria have been proposed along the years and those adopted in this work are described in the followings.

### *I.4.1 SIF evaluation*

There are several approaches to calculate SIFs such as: crack tip opening displacement (CTOD) approach (Citarella, 2010), crack tip stress field approach (Dhondt, 2014) and SIF extraction method from *J*-integral (Citarella, 2010). The *J*-integral, being an energy approach, has the advantage that elaborate representation of the crack tip singular fields is not necessary. This is due to the relatively small contribution that the crack tip fields make to the total *J* (i.e. strain energy) of the body. Therefore, in the present work, the SIFs are extracted from the *J*-integral calculation by leveraging on the method illustrated in the following.

Path independent *J*-integral is defined as:

$$J = \int_S \left(\mathrm{W}\mathrm{n}_1 - \mathrm{t}_\mathrm{j} u_{\mathrm{j},1}\right) \mathrm{dS} \tag{I.1}$$

where $S$ is an arbitrary closed contour, oriented in the anti-clockwise direction, starting from the lower crack surface to the upper one and incorporating the crack tip, $dS$ is an element of the contour $S$, $W$ is the strain energy per unit volume, $\mathrm{n}_1$ is the component in the $\mathrm{x}_1$ direction of the outward normal to the path $S$, and $\mathrm{t}_\mathrm{j} (= \sigma_{\mathrm{ij}} \mathrm{n}_\mathrm{j})$ and $\mathrm{u}_{\mathrm{j},1}$ are the components of the interior tractions and strains, respectively.

J-integral can be related to a combination of the values of $\mathrm{K}_I$ and $\mathrm{K}_{II}$. Ishikawa, Kitagawa and Okamura (Ishikawa, 1980) suggested a simple procedure for doing so and Aliabadi (Aliabadi, 1990) demonstrated that it can be implemented in the DBEM in a straightforward manner.

The application of the *J*-integral to 3D crack problems was presented by Rigby and Aliabadi (Rigby, 1993, 1998) and Huber and Kuhn (Huber, 1993). The application of the 3D *J*-integral to thermoelastic crack problems can be found in dell'Erba and Aliabadi (dell'Erba, 2000).

The *J*-integral for 3D is defined as

$$J = \int_{\Gamma_\rho} \left(\mathrm{W}\mathrm{n}_1 - \sigma_{\mathrm{ij}} \frac{\partial u_i}{\partial x_1} n_\mathrm{j}\right) \mathrm{d}\Gamma =$$
$$= \int_{C+\omega} \left(\mathrm{W}\mathrm{n}_1 - \sigma_{\mathrm{ij}} \frac{\partial u_i}{\partial x_1} n_\mathrm{j}\right) \mathrm{d}\Gamma - \int_{\Omega(C)} \frac{\partial}{\partial x_3} \left(\sigma_{i3} \frac{\partial u_i}{\partial x_1}\right) \mathrm{d}\Omega \tag{I.2}$$

where $\Gamma_\rho$ is a contour identical to $\mathrm{C}_\rho$ but proceeding in an anti-clockwise direction (Fig. I.4). The integral $J$ is defined in the plane $\mathrm{x}_3 = 0$ for any position on the crack front. Considering a traction free crack, the contour integral over the crack faces $\omega$ is zero, instead, with loaded crack faces, as for the LC approach here presented, the contribution of $\int_\omega -\sigma_{\mathrm{ij}} \frac{\partial u_i}{\partial x_1} n_\mathrm{j} \mathrm{d}\omega$ has to be added.

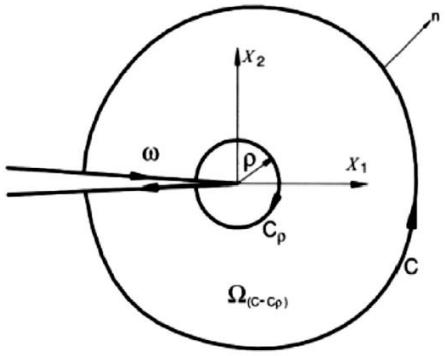


***Figure I. 4*** *Closed path around crack tip (Wilson, 1976).*

For mixed-mode 3D problems, the *J*-integral is related to the three basic fracture modes through the components $J^{I}$, $J^{II}$ and $J^{III}$:

$$J = J^{I} + J^{II} + J^{III} \tag{I.3}$$

Rigby and Aliabadi (Rigby, 1998) presented a decomposition method through which the integrals $J^{I}$, $J^{II}$ and $J^{III}$ in elastic problems can be calculated directly from *J*. Firstly, *J* was divided into two components:

$$J = J^{S} + J^{AS} \tag{I.4}$$

$J^{S}$ and $J^{AS}$ are obtained from symmetric and anti-symmetric elastic fields around the crack plane, respectively. As the mode I elastic fields are symmetric to the crack plane, the following relationship holds:

$$J^{S} = J^{I} \text{ and } J^{AS} = J^{II} + J^{III} \tag{I.5}$$

$J^{II}$ and $J^{III}$ integrals can be calculated from $J^{AS}$ by making an additional analysis on the anti-symmetric fields. Then, when *J*-integral is calculated as sum of the three separated contributions of mode I, II and III, the Stress Intensity Factors $K_{\mathrm{i}}$ can be obtained as:

$$J = J^{I} + J^{II} + J^{III} = \frac{1}{E'}(K_I^2 + K_{II}^2) + \frac{1}{2G}K_{III}^2 \tag{I.6}$$

where $G$ is the shear modulus and $E' = E$ (Young's modulus) for plane stress, or $E' = E/(1-\nu^2)$ for plane strain.

The method for deriving the three separate K values from *J* can be found in (Aliabadi, 2002) or (Rigby, 1998).

### *I.4.2 Kink angle assessment*

Well-established criteria proposed for calculating the crack deflection angles in isotropic media can be: Maximum Tangential Stress (MTS) (Erdogan, 1963), Maximum Energy Release Rate (MERR) (Griffith, 1921, 1924), Minimum Strain Energy Density (MSED) (Sih, 1974), Maximum Principal Asymptotic Stress (MPAS) field (Dhondt, 2001). The MSED criterion has been adopted in the current work and some aspects about this criterion are here provided.

MSED criterion is developed on the basis of the strain energy ($W$) density $dW/dV$ concept ($dV$ is the differential volume). Fracture is assumed to initiate from the nearest neighbour element located by a set of cylindrical coordinates $(r, \theta, \varphi)$ attached to the crack border. The new fracture surface is described by a locus of these elements whose locations correspond to the strain energy function being a minimum. The explicit expression of strain energy density around the crack front tip can be written as:

$$\frac{dW}{dV} = \frac{S(\theta)}{r\cos\varphi} + O(1) \tag{I.7}$$

where $S(\theta)$ is given by

$$S(\theta) = a_{11}K_I^2 + 2a_{12}K_IK_{II} + a_{22}K_{II}^2 + a_{33}K_{III}^2 \quad \text{(I.8)}$$

and

$$a_{11} = \frac{1+\cos\theta}{16\pi G}(3 - 4\nu - \cos\theta) \quad \text{(I.9)}$$

$$a_{12} = \frac{\sin\theta}{8\pi G}[\cos\theta - (1 - 2\nu)] \quad \text{(I.10)}$$

$$a_{22} = \frac{1}{16G}[4(1-\nu)(1-\cos\theta) + (1+\cos\theta)(3\cos\theta - 1)] \quad \text{(I.11)}$$

$$a_{33} = \frac{1}{4\pi G} \quad \text{(I.12)}$$

in which $G$ is the shear modulus of elasticity and $\nu$ is the Poisson ratio. $S/r\cos\varphi$ represents the amplitude of the intensity of the strain energy density field and it varies with the angle $\varphi$ and $\theta$. It is apparent that the minimum of $S/r\cos\varphi$ always occur in the normal plane of the crack front curve, namely $\varphi = 0$. $S$ is known as strain energy density factor and plays a similar role to the SIF.

Such a criterion is based on three hypotheses:

1. the direction of the crack-growth at any point along the crack front is toward the region with the minimum value of strain energy density factor $S$ as compared with other regions on the same spherical surface surrounding the point.
2. crack extension occurs when the strain energy density factor in the region determined by hypothesis $S = S_{min}$ reaches a critical value, say $S_{cr}$.
3. the length, $r_0$, of the initial crack extension is assumed to be proportional to $S_{min}$ such that $S_{min}/r_0$ remains constant along the new crack front.

It can be seen that the Minimum Strain Energy Density criterion can be used both in two and three dimensions. Note that the direction evaluated by the criterion in three-dimensional cases is insensitive to $K_{III}$ since the $a_{33}$ does not have a $\theta$ dependency (eq. I.12).

The crack-growth direction angle is obtained by minimising the strain energy density factor $S(\theta)$ of eq. I.8 with respect to $\theta$. The minimum strain energy density factor $S_{min}$ is then:

$$\frac{dS(\theta)}{d\theta} = 0 \quad -\pi < \theta < \pi \quad \text{(I.13)}$$

$$\theta^*: \{minS(\theta)\} = S_{min} = S(\theta^*) \quad \text{(I.14)}$$

### *I.4.3 Crack-Growth Rate (CGR) assessment*

The simplest fatigue crack-growth law was introduced in 1962 by Paris (Paris, 1961) who linearly connected (in a log-log plot) the crack-growth rate $da/dN$ with the SIF range $\Delta K$ ($a$ is the crack length, $N$ is the number of fatigue cycles) by means of the law:

$$\frac{da}{dN} = C\Delta K^m \tag{I.15}$$

where $C$ and $m$ are constants that depend on the material. $\Delta K$ is defined as $\Delta K = K_{max} - K_{min}$ and it is the SIF variation attained during the fatigue cycling. Being a power law relationship between the crack growth rate during cyclic loading and the range of SIF, the Paris law can be visualized as a straight line on a log-log plot where the x-axis is denoted by the SIF range $\Delta K$ and the y-axis by the crack-growth rate $da/dN$ (Fig. I.6).

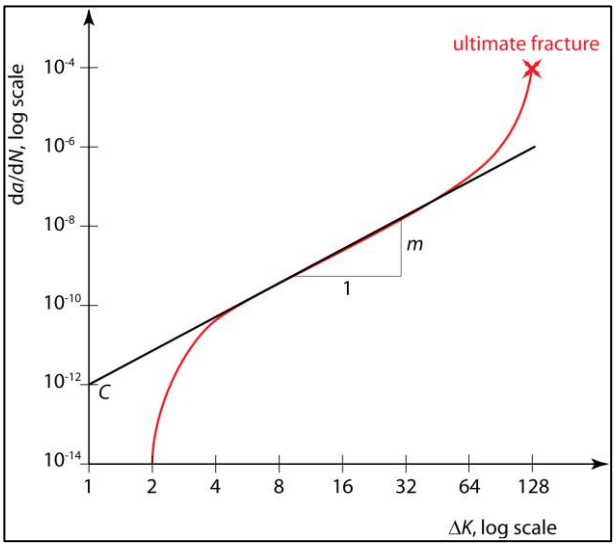


***Figure I. 5*** *Schematic plot of the typical $da/dN$ vs. $\Delta K$ relationship; the Paris law is calibrated to model the linear part of the graph.*

Since Paris discovered such relationship, a lot of research has been devoted to the development of appropriate crack propagation laws. They mostly consist of a Paris range, denoting the linear range, and one or more modifications to cover the drop at the threshold value, the rise to infinity at the critical value and the overall $R$-dependence ($R$ is the stress ratio defined as $R = K_{min}/K_{max}$). An example of such laws is the Forman law (Forman, 1967):

$$\frac{da}{dN} = \frac{C\Delta K^m}{(1-R)K_c - \Delta K} \tag{I.16}$$

where $K_c$ is a further material parameter representative of the critical value of $K$ that leads to the final fracture. A further example is the Walker law (Walker, 1970) that takes into account of the R-dependence in the form of:

$$\frac{da}{dN} = C\left[\frac{\Delta K}{(1-R)^{1-w}}\right]^m \tag{I.17}$$

with $w$ as a material parameter that defines the material sensibility to the mean stress. The most complete crack-growth law is the NASGRO law (NASGRO®, 2002) defined as:

$$\frac{da}{dN} = C\left(\frac{(1-f)}{(1-R)}\Delta K\right)^m \frac{\left(1-\frac{\Delta K_{th}}{\Delta K}\right)^p}{\left(1-\frac{K_{max}}{K_c}\right)^q} \tag{I.18}$$

where the number of material parameters needed to calibrate the law rises up to 8. Further details can be found in (NASGRO®, 2002), however, the law takes into account of the dependencies on the stress ratio $R$, $K_{th}$ threshold value, critical $K_c$ value and small crack propagation phenomenon.

Further crack-growth laws have been proposed in the literature (Dhondt, 2015).

### *I.4.4 Mixed-mode crack-growth*

All the crack-growth laws defined in §I.4.3 are functions of the variability of SIFs $\Delta K$ during the fatigue cycling. However, as described in §I.4.1, three separate $K$ values $(K_I, K_{II}, K_{III})$, representative of the three basic fracture modes, are generally obtained by the *J*-integral decomposition. Therefore, it is necessary to blend together the three distinct $K$ values in one single "equivalent" $K_{eq}$ value to use in a CGR law, this especially when all the three $K$ values are non-negligible (mixed-mode conditions). Some equations to calculate $K_{eq}$ from $(K_I, K_{II}, K_{III})$, calibrated on experimental data, are available in the literature and the most relevant ones are here presented:

- Yaoming-Mi (Mi, 1995) formula:

$$K_{eq} = \sqrt{(K_I + |K_{III}|)^2 + 2K_{II}^2} \tag{I.19}$$

- Sum of squares (Beasy, 2011) formula:

$$K_{eq} = \sqrt{K_I^2 + K_{II}^2 + K_{III}^2} \tag{I.20}$$

- Tanaka (Tanaka, 1974) formula:

$$K_{eq} = \sqrt[4]{K_I^4 + 8K_{II}^4 + \frac{8}{1-\nu}K_{III}^4} \tag{I.21}$$

# Chapter II
# FEM-DBEM benchmark

## *II.1 Introduction*

The work presented in this chapter is based on a benchmarking activity between different numerical approaches to solve a fracture problem. Two FEM codes, ZENCRACK (Zencrack, 2005) and CRACKTRACER3D (Bremberg, 2008, 2009), a DBEM code (BEASY, 2011) and a FEM-DBEM coupled approach have been separately used to calculate Stress Intensity Factors (SIFs), Crack Growth Rates (CGRs) and crack paths for a crack initiated from the outer surface of a shaft undergoing different load cases. The main goal was to get a cross comparison on the results obtained by means of different codes and eventually validate the coupled FEM-DBEM "Loaded Crack" (LC) approach. The comparison was carried out in terms of the so obtained SIFs, kink angles and CGRs and the result are here compared and discussed showing a mutual agreement. Further details can be found in the literature (Citarella, 2017; Giannella, 2017b).

## *II.2 Problem description*

The here presented study case, proposed by Dr. G. Dhondt (MTU Aeroengines) in an attempt to enhance the level of mode mixity against a similar configuration previously analysed (Citarella, 2015a), represents a hub and a hollow shaft, in a symmetric configuration with respect to a mid-plane perpendicular to the shaft axis (Fig. II.1).

Three different load cases have been considered (Fig. II.2):

- "coupled" (Fig. II.2a): consisting of a uniform transversal traction distribution on the shaft end surface, with resultant magnitude equal to 200 kN, and a corresponding point radial force on the hub with same magnitude and opposite direction; in addition, there is a press-fit condition, introducing contact stresses, based on an

interference $\delta = 0.28\,mm$ at shaft/hub contact surface with a static friction coefficient $f_s = 0.6$;

- "shear" (Fig. II.2b): consisting of a uniform transversal force distribution, with resultant magnitude equal to 200 kN, along the hub perimeter line (dotted red line of Fig. II.1b);
- "torque" (Fig. II.2c): consisting of a uniform torque distribution, with resultant magnitude equal to 22.5 kN m, again distributed along the hub perimeter line (dotted red line of Fig. II.1b).

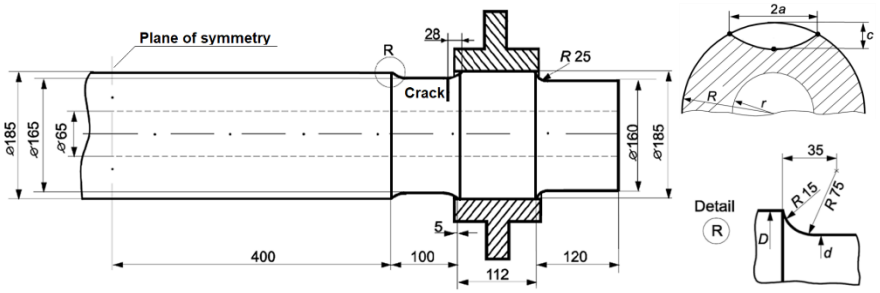


*(a)*

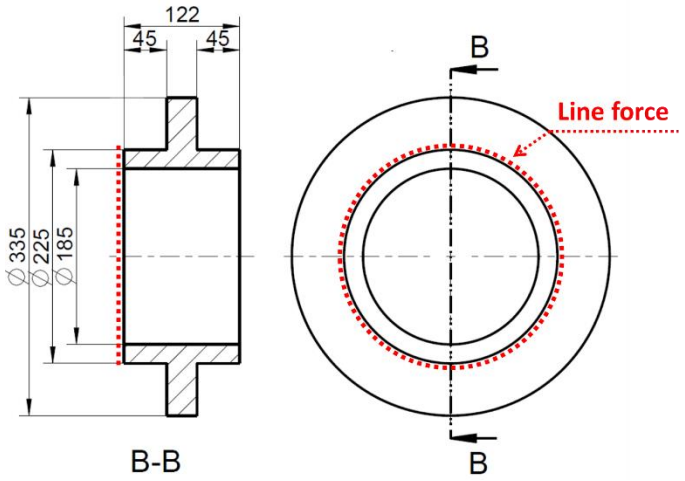


*(b)*

***Figure II. 1*** *Drawings of the (a) shaft with highlight of the crack and fillet radii, (b) hub with the dotted red line representing the loading application zone.*

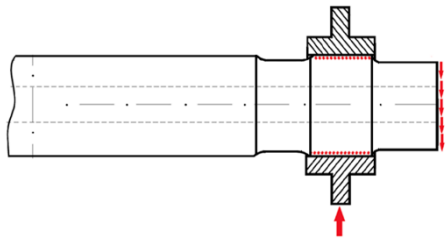


*(a)*

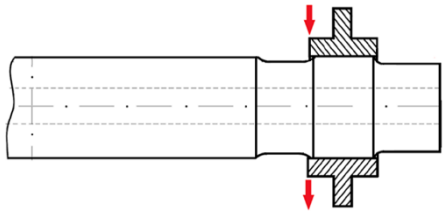


*(b)*

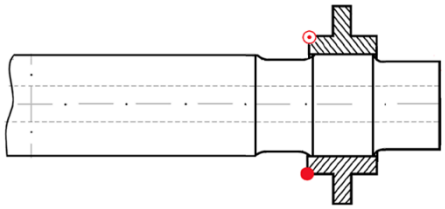


*(c)*

***Figure II. 2*** *Considered load cases: (a) ‘‘coupled”, (b) ‘‘shear” and (c) ‘‘torque”.*

The material is a steel, whose behaviour is assumed being linear-elastic, with the main mechanical and fracture material data listed in Tab. II.1. The geometry of the initially considered part-through crack is an arch of ellipse; the crack is initiated from the external surface of the shaft, having dimensions of $a = 3.8\ mm$ and $c = 1.9\ mm$ (Fig. II.1a).

Four different numerical approaches have been compared to simulate the crack propagation:

- “BEASY” DBEM code: the modelling, the propagation and the stress calculations are performed within the DBEM environment;
- “ZENCRACK” FEM code (hereinafter “ZC”): the stress calculations are performed by the FEM- solver ABAQUS

(ABAQUS, 2011), and both the modelling and the propagation are performed within ZC;

- "CRACKTRACER3D" FEM code (hereinafter "CT3D"): CalculiX (Dhondt, 2016) is used as FE solver whereas the fracture problem is left to CT3D;
- "Loaded Crack" approach (hereinafter "LC"): a FEM code (ABAQUS, 2011) is used to compute the global stress field in the uncracked domain and such results are used to perform the DBEM (BEASY, 2011) fracture analysis on the cracked subdomain (§I.3).

The adopted propagation law is a pure Paris- type (no threshold nor critical value, §I.4.3). The needed Stress Intensity Factors (SIFs) were calculated by using the *J*- integral approach in BEASY (Rigby, 1993, 1998) and ZC, whereas in CT3D, the crack tip stress method was applied (Dhondt, 2001).

Because some of the loadings were truly mixed- mode (especially the torque load case; Marcon, 2014; Berto, 2013; Citarella, 2015b), predictive capabilities for out- of- plane crack-growth were particularly important for this analyses. To this end, the propagation angle predictions were based on: Minimum Strain Energy Density criterion (MSED; Sih, 1974) in BEASY, Maximum Energy Release Rate (MERR) in ZC and, finally, the maximum principal asymptotic stress criterion (Dhondt, 2014) in CT3D.

***Table II. 1*** *Main material data for mechanical and fracture analyses.*

| Parameter | Value |
|---|---|
| E [GPa] | 210 |
| ν [-] | 0.3 |
| C [mm/cycle/(MPa mm)$^{0.5}$)$^{n}$] | 1.23085E-12 |
| m [-] | 2.8 |
| $\Delta K_{th}$ [(MPa mm)$^{0.5}$] | 0 |
| $K_c$ [(MPa mm)$^{0.5}$] | 1E6 |

## *II.3 DBEM modelling*

The DBEM model is made up of two different zones (one for the shaft and one for the hub), with a mesh of quadrilateral 9-noded boundary elements for both functional and geometrical variables.

A part- through crack was inserted on the shaft external surface, see Fig. II.3. After the crack insertion (fully automatic together with the inherent local remeshing with 6 noded triangular boundary elements), the number of elements increased from 2500 to nearly 3100.

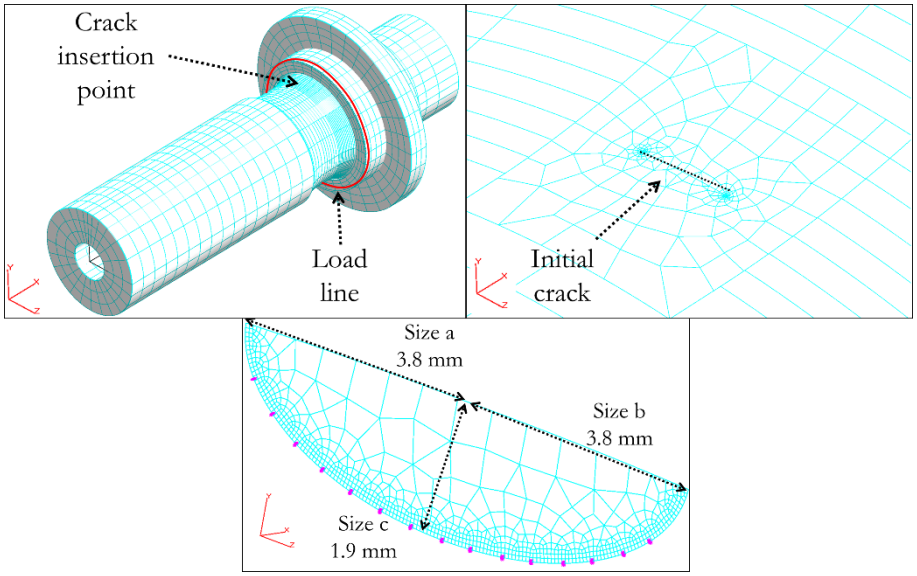


***Figure II. 3*** *DBEM uncracked model with close- up of the remeshed area surrounding the crack insertion point and details of the initial crack geometry with J- paths along the crack front (purple) for the J- integral computation.*

## *II.4 FEM modelling*

The ZC uncracked model (Fig. II.4), created in ABAQUS, consisted of three different volumes: one for the shaft without crack-growth domain, one for the hub and the last for the crack-growth domain. A mesh of 8 noded brick elements with reduced integration was used throughout the model except for the crack-growth domain (i.e. the "large" elements shown in Fig. II.4) that was meshed with 20- node brick elements with full integration. The uncracked FEM model, with nearly 194,000 elements, was then processed by the ZC Graphical User Interface (GUI), substituting each "large" brick with a crack block selected from the ZC crack block library (Zencrack, 2005). In this work, the crack blocks belong to the L02 family and have a maximum of 12 ring contours delimitating the user defined crack front. Each crack block includes nearly 4000 elements, enclosing a rosette of fully quadratics and collapsed quarter- point elements surrounding the crack tip. Loads and boundary conditions were applied in the same way as for the DBEM model (§II.3).

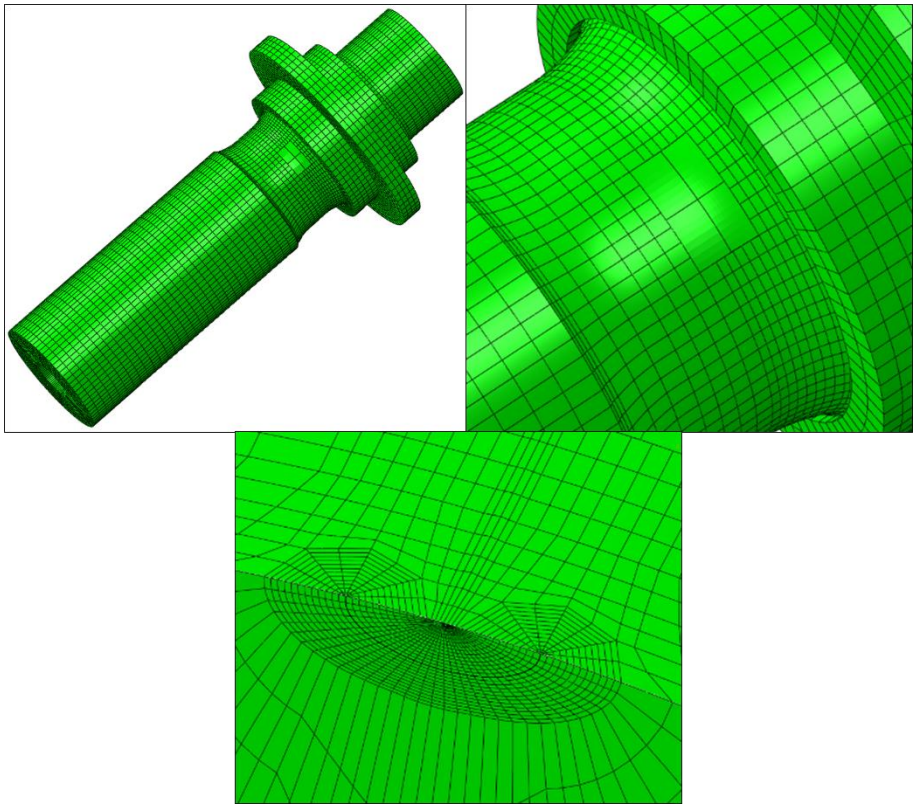

***Figure II. 4*** *ZENCRACK (ZC)/ABAQUS uncracked model with highlight on the brick elements that are subsequently substituted with crack blocks.*

The CT3D uncracked model (Fig. II.5) was created with CalculiX GraphiX (Dhondt, 2016) by using 20- node brick elements with reduced integration. The yellow elements in the figure constitute the domain, which is the set of elements that is remeshed to accommodate the crack. Fig. II.5 shows also such domain after remeshing: a flexible tube was introduced along the crack front and filled with 20 noded hexahedral elements with reduced integration, whereas, quadratic (10 noded) tetrahedral elements were used to fill the remaining space. The hexahedral mesh in the tube and the hexahedral mesh in the structure outside the domain are connected with the tetrahedral mesh by using linear multiple point constraints. At the crack tip, collapsed quarter-point elements are used to enforce the correct linear elastic stress and strain singularity.

The boundary conditions for the coupled load case consisted of a suppression of all degrees of freedom in the geometrical symmetry plane and a true surface- to- surface contact with a static friction coefficient of 0.6, a normal contact stiffness of 10 MN/mm3, and a stick stiffness of 0.1 MN/mm$^3$.

For the shear loading, the boundary conditions were the same as for bending but, in addition, a tied contact between hub and shaft was adopted (no

relative motion possible between shaft and hub). Finally, for the torsion loading, the displacements in axial and circumferential directions in the geometrical symmetry plane were set to 0 and tied contact was applied between the shaft and the hub.

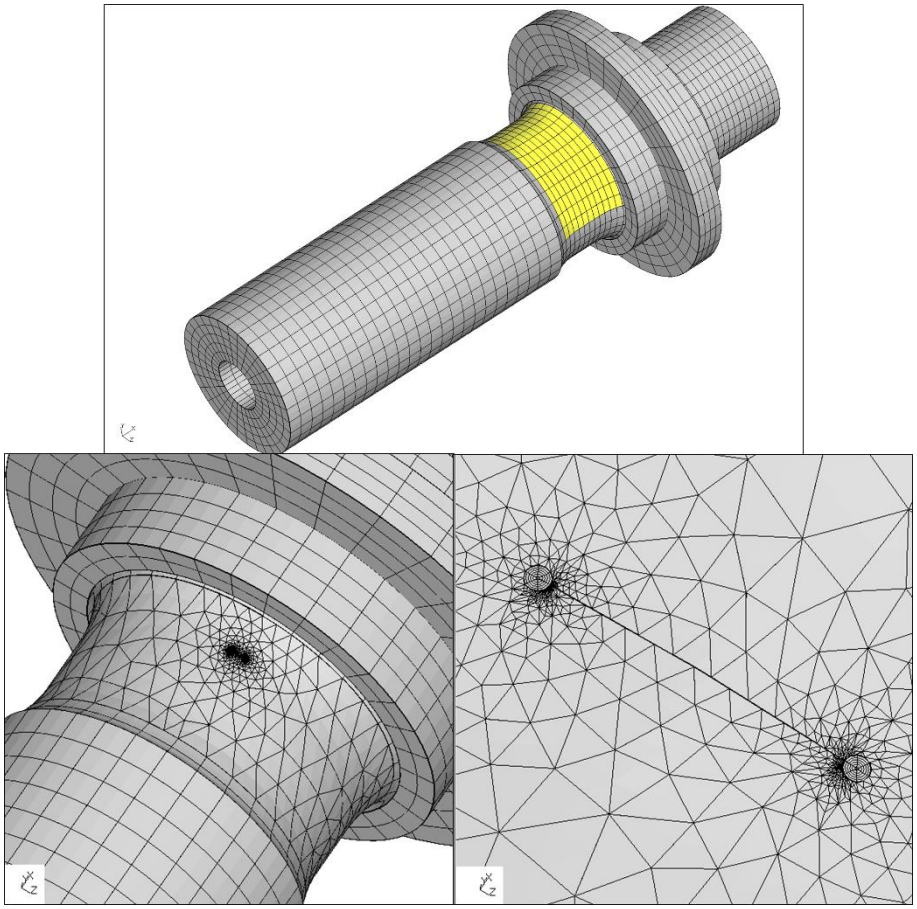

***Figure II. 5*** *CRACKTRACER3D (CT3D)/CalculiX uncracked model with the subsequent cracked mesh and details of the crack.*

## *II.5 FEM-DBEM modelling*

The global FEM model, similar to that shown in Fig. II.4, was also considered as the global model from which to extract a DBEM submodel useful to work out the fracture simulations. The adopted approach for the submodelling strategy was the Loaded Crack (LC) (§II.3) approach in which, only the crack face loads were considered as driving force for the whole crack-growth. Such DBEM crack face loads come from the FEM model of Fig. II.4

in which, the large crack elements were substituted with a fine mesh. In particular, the stresses along the virtual surface traced by the crack have to be evaluated with the highest possible precision, because they represent the driving force for the following DBEM crack propagation.

When using such an LC approach, the FEM mesh in the cracked area has to be very fine to retrieve accurate tractions to be applied on the DBEM crack faces. For this reason, a FEM submodel (Fig. II.6a), containing a small portion of the shaft, was extracted from the FEM global model to accurately calculate the local stress field. Such submodel, containing only the volume surrounding the crack insertion point, has size and mesh refinement capable to guarantee a very high accuracy when evaluating the stress field in the neighbourhood of the crack (higher than that provided by the global model). To get the needed precision, especially for the torque load case, it has been necessary to strongly refine the FEM submodel mesh. This was due to the high kink angles predicted for the torque load case (nearly 90° for the initial propagation steps) that required small crack advances per step and consequent heavy DBEM mesh refinements.

Subsequently, a BEM submodel (Fig. II.6a) is created containing the zone surrounding the crack initiation point (the crack is not yet modelled and that is why the DBEM formulation is not yet enforced). In addition to the FEM stresses, applied as tractions on the crack faces (Fig. II.6b), springs of negligible stiffness (in purple in Fig. II.6a) are applied to a few BEM elements in order to prevent rigid body motion (nodal rigid body constraints are prevented in case of crack propagation). Due to the loading conditions consisting of just a self-equilibrated load, a large part of the DBEM cracked submodel (now the crack has been introduced with automatic remeshing in the surrounding area) turns out to have a null stress field. For this reason, the fracture problem can be analysed considering a very small portion of the entire model, with inherent decrease of the needed computational effort.

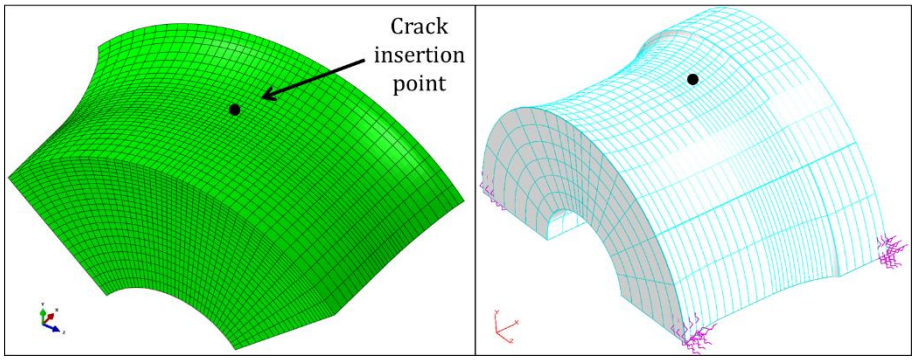


*(a)*

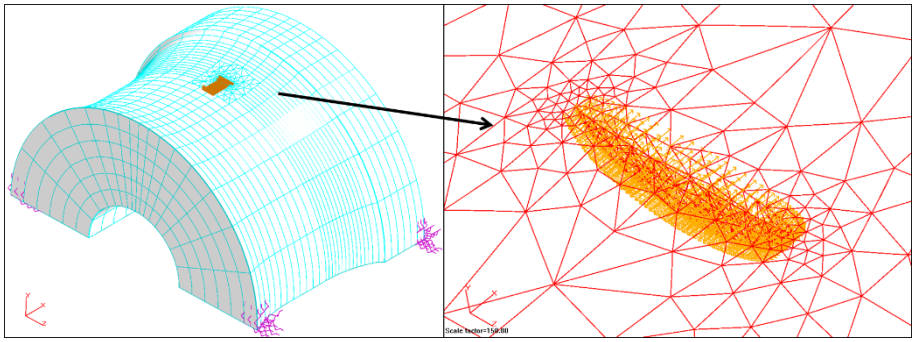

*(b)*

***Figure II. 6*** *(a) FEM and DBEM submodel used for the FEM-DBEM approach; (b) DBEM submodel after that the crack has been inserted and loaded.*

The FEM submodel of Fig. II.6a, when used for the coupled and shear load cases, comprised nearly 25,000 hexahedral elements whereas, for the torque load case, comprised nearly 130,000 hexahedral elements.

A preliminary study was aimed at assessing the minimum needed dimensions of the DBEM submodel, useful to guarantee a complete vanishing of stresses from the crack area to the boundaries. Such uncracked DBEM model comprises nearly 1200 linear elements and this number rises up to nearly 1800 when the initial crack is inserted. The remeshing zone and the crack faces are discretised with 9 noded quadratic elements whereas 4 noded linear elements are used for the bulk of the remaining mesh.

## *II.6 Results*

A crack-growth was simulated for each of the four abovementioned approaches in correspondence of three loading conditions. Results are here

compared and discussed in terms of SIFs for the initially considered crack and in terms of CGRs obtained during the crack-growth simulations. No stress-displacement fields were available for comparison between all the methodologies since the FEM-DBEM LC approach does not allow to replicate the FEM fields in the DBEM environment: only the crack tip singularities can be correctly captured as stated by the superposition principle. Namely, the DBEM solution aims just at the appropriate characterization of the crack tip stress behaviour in order to correctly compute SIFs, but it cannot provide a realistic stress scenario throughout the domain.

In summary, for the LC approach, FEM stresses were applied as tractions to the crack faces of the DBEM submodel and then SIFs along the crack front were obtained by using the *J*-integral. All the so calculated SIFs are compared in the Fig. II.7 showing a very good agreement between the four methodologies and three load cases.

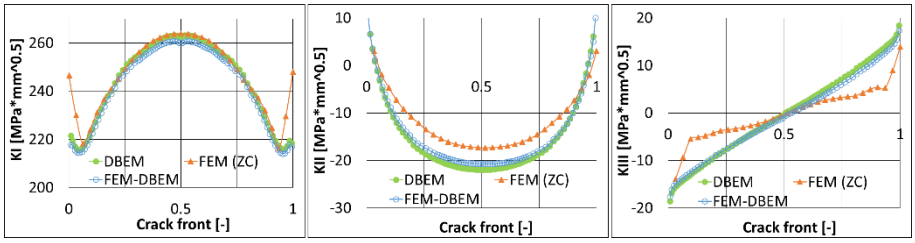


*(a)*

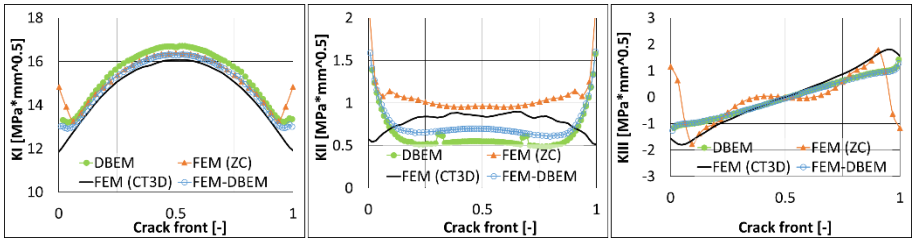


*(b)*

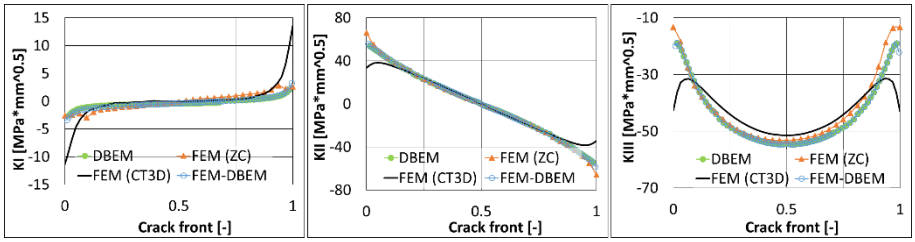


*(c)*

***Figure II. 7*** *SIFs calculated by the considered methodologies for load cases: (a) coupled, (b) shear and (c) torque; X-axis is the normalised abscissa drawn along crack front.*

Crack propagation simulations were run considering a 0-max fatigue load cycle with the maximum value corresponding to the loads defined in §II.2. The simulations were all performed through a step-by-step growth of the crack, involving a remeshing and a stress field evaluation (with corresponding SIFs) at each crack-growth increment. The codes used in this work calculate the kink angles in different ways: MSED by BEASY, MERR by ZC, and maximum principal asymptotic stress criterion by CT3D.

A pure Paris' law (§I.4.4; Paris, 1961) was adopted to predict the Crack Propagation Rates for all the codes:

$$\frac{\mathrm{da}}{dN} = C\Delta K_{eq}^{m} \tag{II.1}$$

where the material parameters $C$ and $m$ are listed in Tab. II.1. $\Delta K_{eq}$ is an equivalent SIF, calculated by different combinations of mode I, II, and III SIFs, depending on the considered code.

In particular, for the DBEM and FEM-DBEM approaches here adopted, the procedure based on the decomposition of the elastic field into respective symmetric and antisymmetric mode components, available in §I.4.1 (Rigby, 1993, 1998), was adopted to obtain the three separate $K_I$, $K_{II}$ and $K_{III}$ values. Then, the $\Delta K_{eq}$, in case of $R = 0$, can be obtained by means of the Tanaka formula (§II.4.4) here reported:

$$K_{eq} = \sqrt[4]{K_I^4 + 8K_{II}^4 + \frac{8}{1-\nu}K_{III}^4} \tag{I.19}$$

Regarding the ZC code, the total energy release rate was used for calculating the $K_{eq}$:

$$K_{eq} = \sqrt{\left[\frac{E}{1-(\alpha\nu)^2}G_{eff}\right]}, \tag{II.2}$$

where α is a measure for the stress state taking values between 0 and 1 (0 for plane stress state and for plane strain state) whereas $G_{eff}$, in case of $R = 0$, corresponds to:

$$G_{eff} = \frac{B}{E}(K_I^2 + K_{II}^2) + \frac{1}{2G}K_{III}^2, \tag{II.3}$$

where $B = 1 - \nu^2$ for plane strain and $B = 1$ for plane stress, and $G$ is the shear modulus.

Finally, the calculation of the equivalent SIF is more cumbersome in the CT3D code. Using the K- values of the three modes, the asymptotic stress field is considered at each position along the crack front; the $K_{eq}$ is then defined as the principal self- similar stress evaluated in correspondence of the deflection angle φ for which the principal plane contains the crack tip. The corresponding principal plane dictates also the propagation direction. For any details, the reader is referred to the paper by Dhondt (Dhondt, 2014).

Using the crack- size definitions in Fig. II.8, the graphs of the crack size versus number of cycles are shown in Fig. II.9 for all the simulations. Based on the K- values along the initial crack front, it was possible to envisage that both the coupled and shear load cases lead to in-plane crack-growth. The calculations confirmed this. Looking at the curves in Figure II.9, the $c/a$ ratio changes for the coupled case from 0.5 to about 0.75, i.e., the form of the crack becomes less skewed during the propagation. This, too, was to be expected because the initial K- values in the middle of the crack front were much higher than those at the free surface. For the torque loading, the mode I is clearly dominated by mode II and especially mode III. Therefore, out- of- plane crack-growth was expected to be important in both cases.

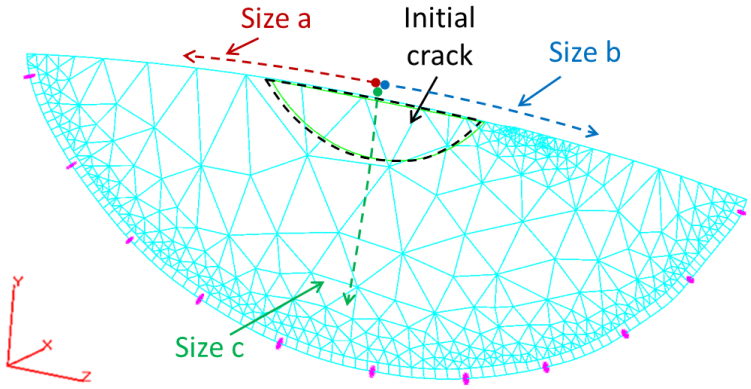


***Figure II. 8*** *Crack size definitions.*

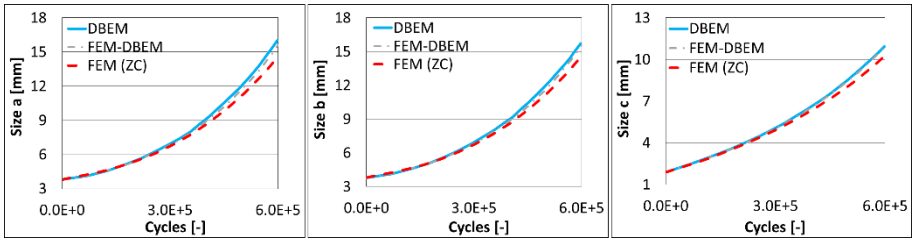


*(a)*

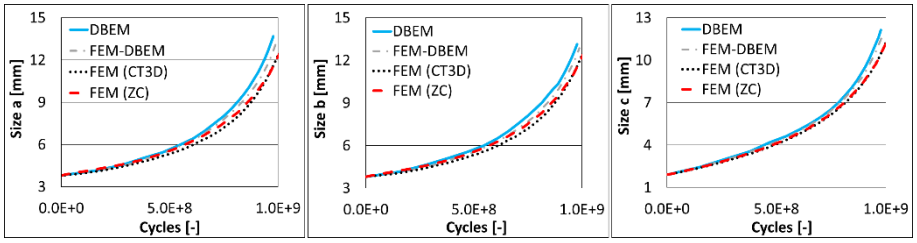


*(b)*

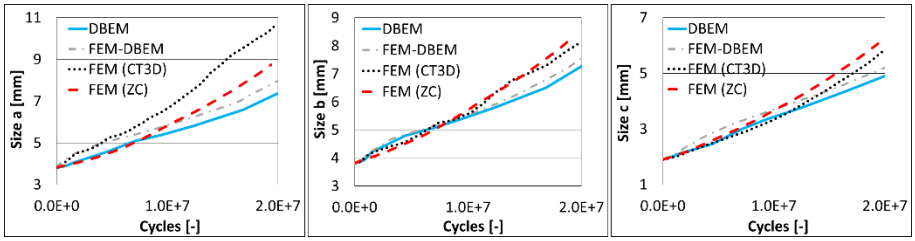


*(c)*

***Figure II. 9*** *Plots of crack sizes vs. total fatigue cycles for the load cases of: (a) coupled; (b) shear; (c) torque.*

Runtimes for performing the various crack propagation simulations were compared between the four codes. The average runtimes calculated for one step of crack advance are listed in Tab. II.2. An average value was calculated because during the propagation, the number of elements needed to discretise the crack increases and consequently so do runtimes.

Tab. II.2 clearly shows that the FEM-DBEM LC approach takes much lower time then that required for the same calculation using DBEM and the ratio is even more advantageous if compared to a FEM code. This was expected since the LC model to handle is smaller than the others and the kind of analysis is generally simpler (pure stress analysis). In addition, a high accuracy is guaranteed.

***Table II. 2*** *Runtime for the entire propagation for the coupled load case for the various adopted approaches.*

| Code | Runtime [min] |
|---|---|
| DBEM | 1360 |
| FEM-DBEM | 231 |
| FEM (ZC) | 500 |

## *II.7 Remarks*

Four approaches were applied to three mixed- mode crack propagation test cases. Although the codes use completely different methods to modify the mesh at the crack tip and to calculate the stresses, the SIFs, the kink angles, the CGRs and the shape of the resulting crack are quite similar. The most advanced approach appeared to be the FEM-DBEM one since such submodelling strategy allows to get an accurate SIF assessment along the crack front together with runtimes much lower than those needed by pure DBEM and FEM approaches. Moreover, the LC approach allows to circumvent some of the inaccuracies inherent to the “classical” submodelling

implementations. One of the reasons is that, with the LC approach, the loads on the submodel (namely on the crack faces), are rigorously updated for each step of the incremental crack-growth.

# Chapter III
# FEM-DBEM application on an aeroengine turbine

## *III.1 Introduction*

A realistic application of two distinct approaches based on the Dual Boundary Element Method (DBEM) to solve a Fracture Mechanics (FM) problem on a GE-AVIO aeroengine turbine is presented in this chapter. A "Fixed Displacement" (FD) and a "Loaded Crack" (LC) FEM-DBEM submodelling approaches have been used to simulate the thermo-mechanical fatigue crack-growth of an initial metallurgical defect as detected on a statoric segment. The results in terms of SIFs and CGRs are here compared showing that the LC approach allowed to overcome the inaccuracies that inevitably arise when using classical submodelling strategies such as FD (or similarly "Fixed Load", FL).

## *III.2 Problem description*

Design of turbine rotor blades and vanes for aircraft engines asks for cutting-edge modelling capabilities, because such structural components are subjected to high temperatures, complex mechanical loads, corrosive environment and long expected lifetimes, to not mention the catastrophic consequences of a structural failure.

Turbine operating conditions vary drastically from take-off to landing phases of a common aircraft operating cycle, with temperatures reaching up to 1300 K, imposing severe thermo-mechanical fatigue loadings on the stressed materials. Extreme temperature gradients and transients induce cyclic thermal-stresses on the turbine vanes and consequent Thermo-Mechanical Fatigue (TMF) conditions. It is therefore of utmost importance to accurately evaluate the impact of potential detected defects on these components.

To this aim, two FEM-DBEM submodelling strategies have been adopted in this work to solve a realistic fracture problem in an aircraft engine turbine stage. As proved in recent works, FEM and DBEM methods can efficiently work together when tackling large structures (Citarella, 2013, 2014), residual stresses generated by plastic deformations (Citarella, 2014, 2016a, 2016c; Carlone, 2015) or load spectrum effects (Citarella, 2009).

The two procedures are tested on the crack scenario detected on a turbine vane of a commercial aircraft engine. The load spectrum driving the fatigue crack propagation is representative of a GAG (ground-air-ground) cycle. The range of Stress Intensity Factors ($\Delta K$) is used as the crack driving force and Crack Growth Rates (CGRs) are calculated by using a Paris' law (§I.4.3; Paris, 1961) calibrated by material fatigue crack-growth data obtained at the temperature of interest.

The FEM and DBEM used codes are ANSYS (ANSYS, 2007) and BEASY (BEASY, 2011) respectively.

## *III.3 FEM modelling*

The global FEM model considered in the analyses is representative of a statoric segment, made of six airfoils, of a low pressure turbine stage of a commercial aircraft engine. It was modelled considering a typical turbine blade superalloy, with mechanical and thermal isotropic material properties, whose variations against temperature are illustrated in Fig. III.1. Fluid pressure was modelled as a mechanical load, applied on both sides of the airfoils, in addition to the temperature scenario, previously calculated by thermo-fluid-dynamic analyses (Fig. III.2a). In addition, cyclic symmetry boundary conditions were enforced on the casing that couples with the statoric segment, in order to simulate the circumferential periodicity of the entire stage (Fig. III.2b). Surface to surface contacts were applied on the interfaces between statoric hooks and casing. Thermal and mechanical loads applied on the global model were representative of the most severe conditions for an aircraft engine during its mission, namely, those reached at take-off. As a matter of fact, during the take-off, there is the need for the maximum boost of the engines and, consequently, vane temperatures get the highest magnitudes and the highest gradients with consequent enhancement of the so generated thermal-stresses.

In correspondence of the boundary conditions related to the most critical mission point, a tangential displacement distribution was evaluated (Fig. III.3a). Due to a combination of mechanical and thermal cyclic stresses, fatigue cracks can nucleate, most likely from locations with highest stresses, localized in-between airfoils and casing (Fig. III.3b, the figure shows also the crack insertion point for the subsequent fracture analyses).

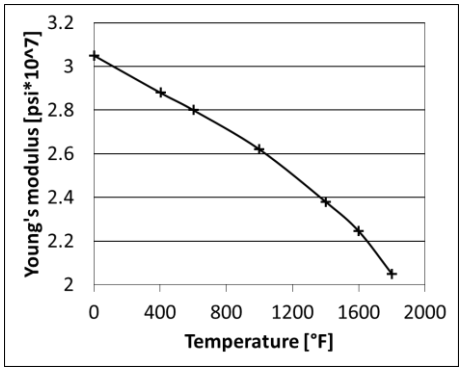


*(a)*

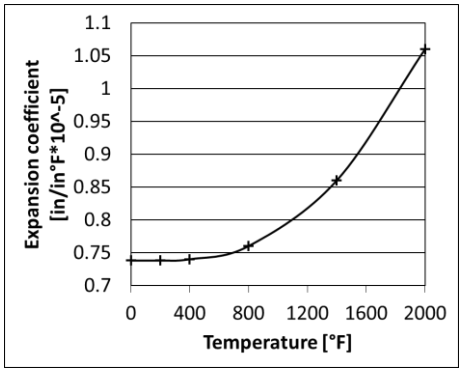


*(b)*

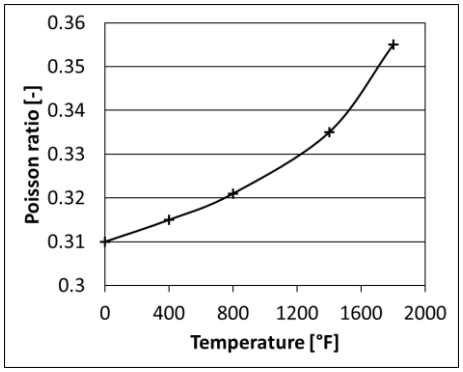


*(c)*

***Figure III. 1*** *Material properties vs. temperature for the considered superalloy: Young's modulus (a), thermal expansion coefficient (b) and Poisson's ratio (c).*

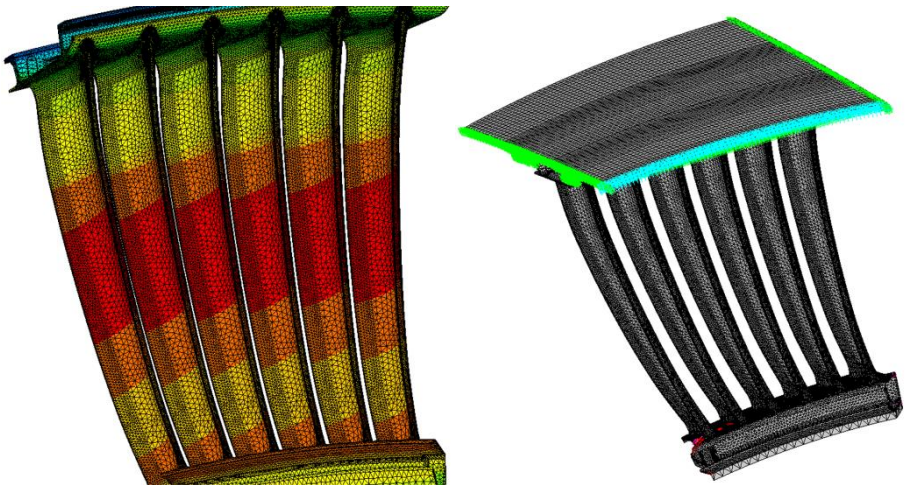

*(a)* *(b)*

***Figure III. 2*** *FEM model: (a) thermal scenario and (b) cyclic symmetry boundary conditions (highlighted in green).*

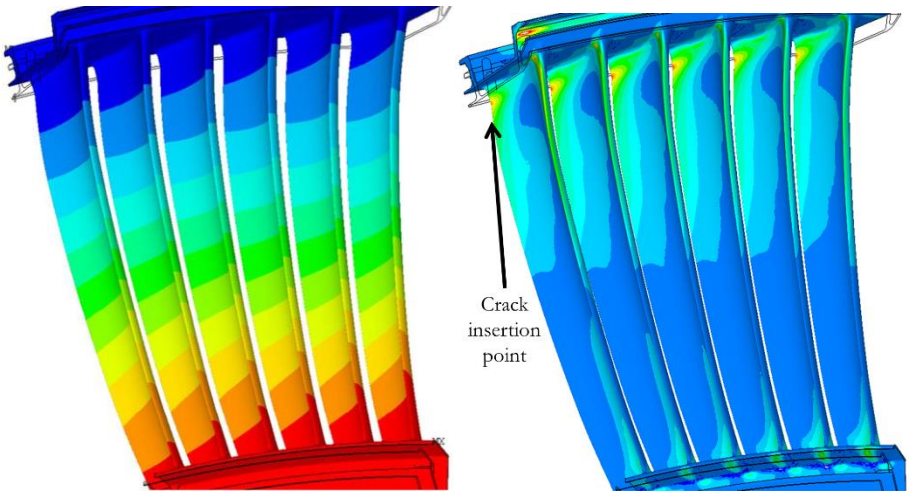


*(a)* *(b)*

***Figure III. 3*** *Tangential displacements (a) and max principal stresses (b) on the statoric segment.*

## *III.4 Metallographic post-mortem investigation*

A post-mortem metallographic investigation was developed on the damaged vane, in order to assess the causes of the engine failure (Fig. III.4).

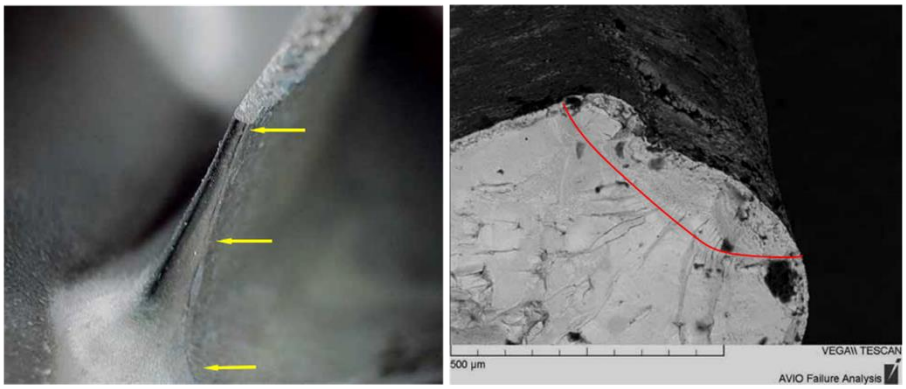


*(a)* *(b)*

***Figure III. 4*** *Segment affected by fatigue failure: (a) damaged airfoil with highlight (yellow arrows) of the undesired double radius on the trailing edge; (b) estimated initial crack front (red line).*

The affected airfoil was the N. 6 of a statoric segment of the fifth low-pressure turbine stadium. The fatigue crack nucleation (Fig. III.4b) was likely caused by:

- a combined effect of two initial manufacturing defects: an irregular trailing edge profile (double radius visible in Fig. III.4) and a metallurgical discontinuity (enclosed by the red line in Fig. III.4b);
- an operational anomalous stress intensification at the crack location caused by off mission envelope test conditions.

## *III.5 DBEM submodelling approach*

From the mission profile of Fig. III.5a, a simplified thermo-mechanical fatigue load cycle was extracted, with its maximum value corresponding to the take-off phase and its minimum value corresponding to the engine shut-off (zero load; Fig. III.5b).

Mechanical, thermal and fatigue properties for the considered superalloy, evaluated at an average temperature of the DBEM submodel, are listed in Tab. III.1. In detail, the calibration of the Paris' law (I.4.3) used to calculate the CGRs was performed at the average submodel temperature. The DBEM submodel cannot allow for the spatial variability of the material properties caused by the gradients, consequently, uniform material properties were used as evaluated in correspondence of the average submodel temperature. Nevertheless, for the analysed problem, the impact of such approximation on the final results (e.g. SIFs along the crack front) turns out to be negligible due to the limited temperature variation in the very small submodel adopted for the analyses.

SIFs were calculated resorting to the *J*-integral approach (Wilson, 1979; Rigby, 1993; Dell'Erba, 1998, 2001) and the crack path assessment is based on the Minimum Strain Energy Density (MSED) criterion (Sih, 1974). In this work, a comparison on different crack path criteria was not provided because the crack evolves under nearly pure mode I, so that, the crack kinking assessment did not represent a critical step.

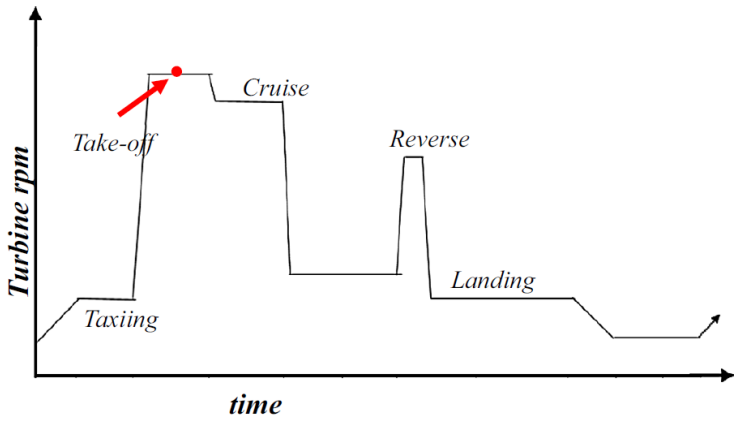


*(a)*

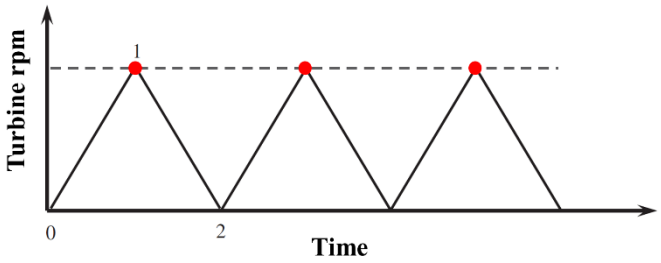


*(b)*

***Figure III. 5*** *(a) Realistic engine mission profile and (b) its simplified profile adopted in this work.*

A small portion of the whole FEM model (Fig. III.2) was extracted by means of a spherical cutting domain and converted in a DBEM submodel by a skinning procedure (BEASY software provides an interface utility capable to enforce automatically such an extraction). Then, a crack was introduced and propagated taking advantage of the automatic remeshing capabilities of the adopted DBEM code.

In particular, two DBEM submodels (Fig. III.7) were cut by two spherical domains, both centred in the same position, the crack initiation point of Fig. III.3b, but having different sphere radii of $r = 1$ in. and $r = 0.3$ in. Such submodels were imported in the DBEM environment in order to assess the

minimum submodel size capable to ensure insensitivity of boundary conditions against the crack-growth results. FD submodel was loaded with displacement boundary conditions at subdomain cut surfaces (fluid pressure on the airfoils was negligible) whereas LC submodel was loaded with only tractions on crack faces.

Using FD procedure, then without allowing for an update of boundary conditions during the crack-growth, it turns out mandatory to cut a submodel sufficiently larger than crack sizes. Such drawback can be circumvented by resorting to LC approach, where the submodel minimum size can be much lower, with consequent reduction of computational effort. As a matter of fact, having applied just a self-equilibrated load on the crack faces, it is sufficient to enclose in the sphere cut just that restricted volume portion surrounding the crack affected by non-null stresses, as shown in the following.

***Table III. 1*** *Mechanical, thermal and fatigue properties at the sub-model average temperature.*

| Parameter | Value |
|---|---|
| Young's modulus [psi] | 23.5E6 |
| Poisson' ratio [-] | 0.337 |
| Thermal expansion coeff. [in./(in.*°F)] | 8.75E-6 |
| Reference temperature [°F] | 77 |
| Paris' law coeff. C [$psi^{1-n}/in.^{n/2}$] | 2.62E-24 |
| Paris' exponent m [-] | 4.37 |
| Threshold limit $K_{th}$ [$psi*in^{0.5}$] | 7410 |
| Fracture toughness $K_c$ [$psi*in^{0.5}$] | 46153 |

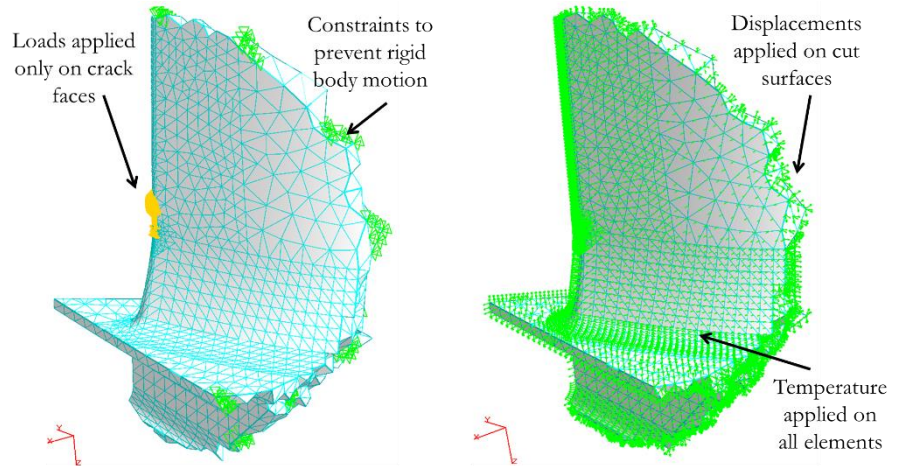


***Figure III. 6*** *Considered loading strategies for DBEM analyses: (a) LC and (b) FD; model for LC comprises the self-equilibrated load on the crack face elements and few constraints to prevent rigid body motion; model for FD comprises temperature on all the elements and displacement field on all the cut surface elements.*

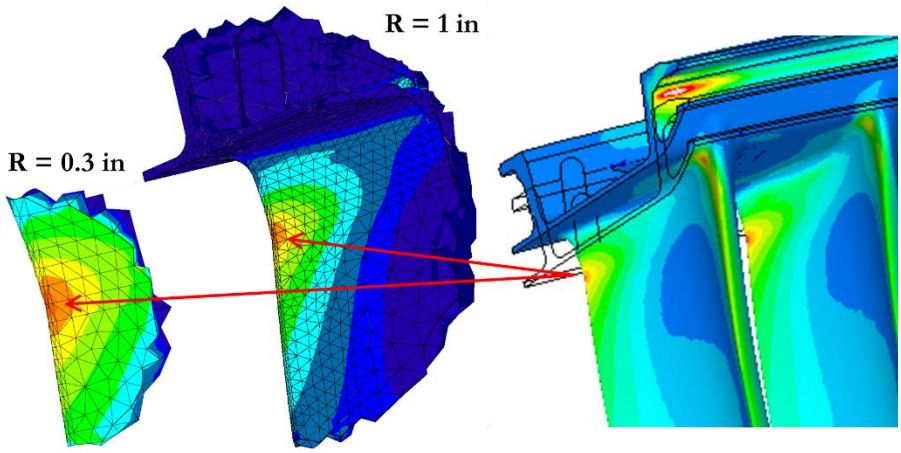


***Figure III. 7*** *Max principal stresses before crack introduction on the two DBEM submodels used for FD approach; highlight of the crack insertion position.*

## *III.6 Results*

The first goal was to assess the minimum required submodel size "compatible" with the boundary conditions that were updated or not during crack-growth for LC and FD respectively. In more details, submodel boundary conditions for both FD and LC approaches come from the FEM analysis of the uncracked global model but, for the FD approach, this represents an element of approximation. In fact, the displacement boundary conditions applied on the cutting surfaces should, in principle, be updated at each step of crack advance, to allow for the submodel stiffness variation when solving the global model. On the contrary, with the LC approach, the self-equilibrated tractions applied on both faces of the crack are correctly extracted from an uncracked body solution, as rigorous dictated by the superposition principle implementation (§I.2). Moreover, such tractions are updated step-by-step because new crack surfaces are continuously created and loaded during the crack-growth simulation. Thus, for LC approach there is no need to guarantee a submodel much larger than the crack extension, being sufficient to enclose the volume surrounding the crack with non-zero stresses; such stress ''fading distance" can be very short because of a self-equilibrated load applied to the model.

The crack representing the initial detected defect (red line in Fig. III.4b) was modelled and inserted in both LC and FD DBEM submodels. Introducing the crack into DBEM submodels, with the inherent automatic remeshing of the cracked surroundings, two different stress scenarios came out from FD and LC approaches (Fig. III.8): the former produces a realistic stress scenario throughout the whole DBEM submodel whereas the latter is meaningful only for the SIFs evaluation. Hence, a comparison between the two methodologies can just involve SIFs along the crack front and, therefore, the CGRs and kink angles that are directly connected to the SIFs calculation.

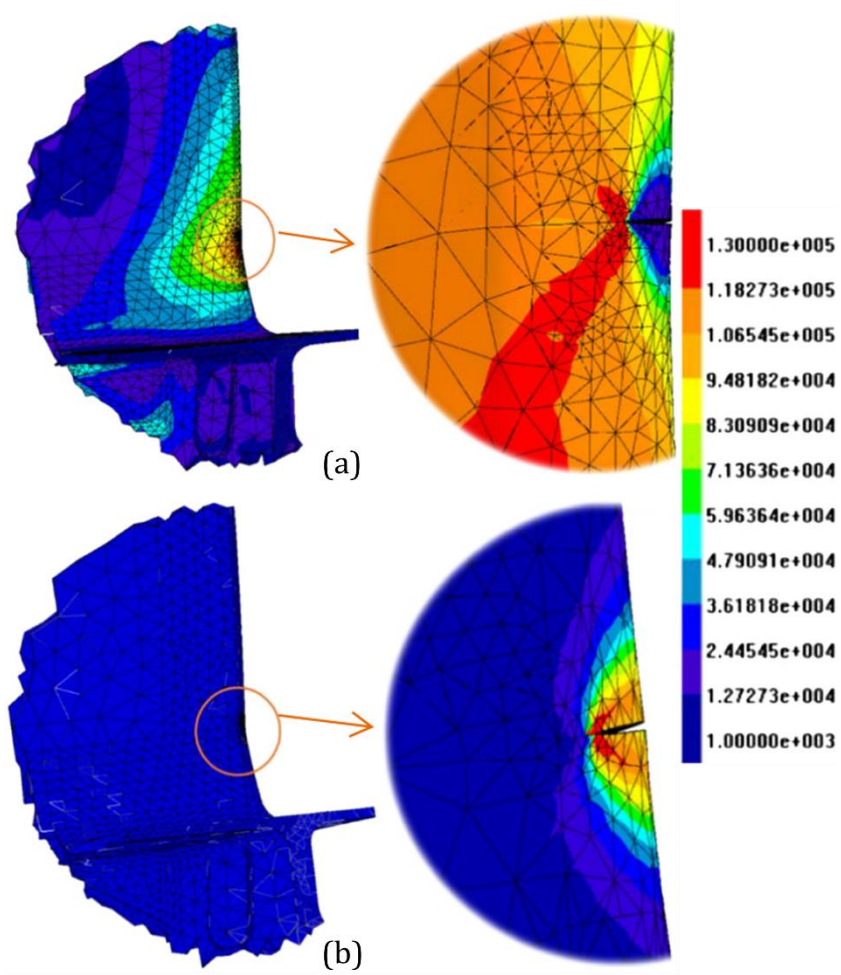


***Figure III. 8*** *Von Mises stresses [psi] for the initial cracked FD (a) and LC (b) models, with close-up of the cracked area (cutting sphere radius R = 1 in.).*

A convergence study (Fig. III.9-10) was performed for both the FD and LC methodologies, varying the submodel size and the mesh refinement on and nearby the crack (Fig. III.9), in order to benchmark the respective convergence rates and computational efficiencies. Analysing the so obtained SIFs, it was possible to observe a high convergence rate of LC methodology (Fig. III.10a), rapidly providing a convergent SIF distribution along the crack front even for coarse meshes, i.e. with high crack front element size (hereinafter "cfes", BEASY, 2011) values. On the contrary, the FD methodology needed strong mesh refinements (Fig. III.10b) to get convergent results but, anyhow, perfectly coincident SIFs could not even be obtained since too fine meshes

were needed. Fig. III.10 shows the mode I SIFs but the same behaviour was obtained also for $K_{II}$ and $K_{III}$.

However, comparing the results provided by the two methodologies in correspondence of the initial cracked configuration (Fig. III.10), it was possible to guarantee the correctness on the implementation of the proposed LC approach.

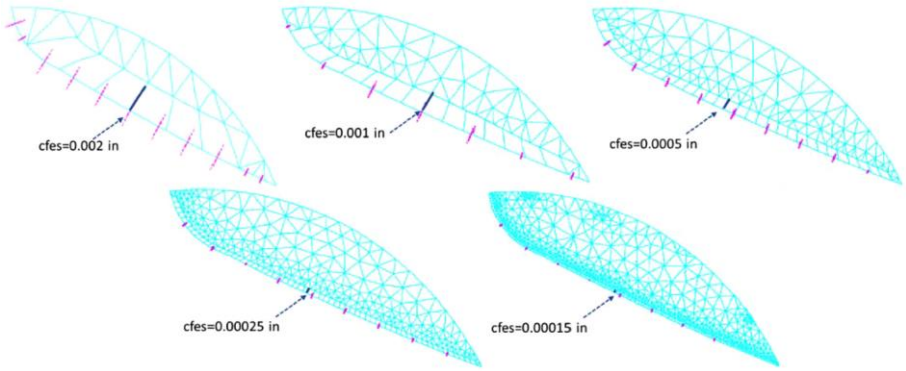


***Figure III. 9*** *Different meshes on the crack face, as used for the convergence study.*

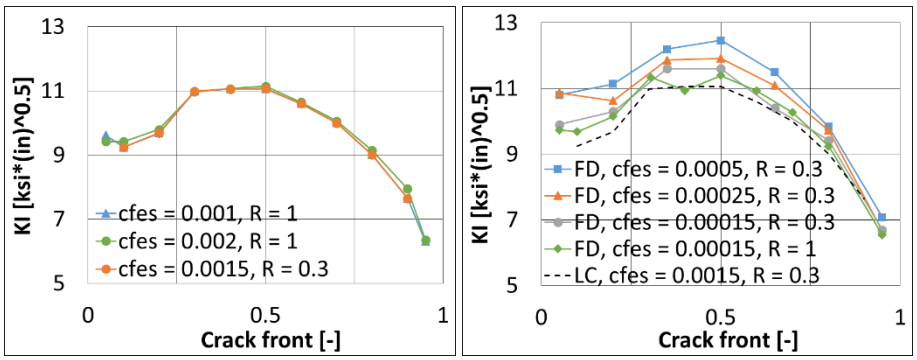


*(a)* *(b)*

***Figure III. 10*** *Different meshes on the crack face, as used for the convergence study between (a) LC and (b) FD methods; X axis is the normalised abscissa drawn along the crack front.*

Crack size vs. cycles, calculated with LC and FD methodologies are compared in Fig. III.11. Crack propagation has been stopped when the maximum equivalent SIF $K_{eq}$, calculate by means of the eq. I.19:

$$K_{eq} = \sqrt{(K_I + |K_{III}|)^2 + 2K_{II}^2} \tag{I.19}$$

and, in this case, nearly coincident with $K_I$ due to the reduced level of mode mixity, reaches 96% of fracture toughness $K_c$.

Due to the complex shape of the crack, Fig. III.11 reports on the y-axis an equivalent crack length defined as.

$$Eq.Length = \frac{Crack\ area}{Crack\ front\ length} \quad \text{(III.1)}$$

Convergent crack propagation results related to the classical FD approach could not be calculated due to the excessive mesh refinement needed and the prohibitive runtimes.

LC SIFs for both small and large submodels are nearly overlapped along the whole propagation and consequently the same holds true for the crack size vs. cycles (Fig. III.11a). On the contrary, SIFs from FD approach are overlapped for small and large submodels just for the initial crack propagation steps, i.e. when the DBEM cut surfaces are still sufficiently far from the advancing crack, whereas, a progressive divarication between the curves of crack size vs. cycles occurs as the crack grows (Fig. III.11b).

In conclusion, the performed analyses clearly show that the LC approach allows to consider a smaller submodel than that needed by the FD approach without affecting the accuracy, with a consequent benefit in terms of runtimes. Indeed, runtimes for the solution of the initial crack scenarios (step 0) are compared in Tab III.2, clearly showing the advantage of using LC instead of FD. In order to obtain the same accuracy on SIFs assessment, the adopted meshes are:

- crack front element size “cfes” equal to 0.00015 in. for FD model;
- crack front element size “cfes” equal to 0.002 in. for LC model.

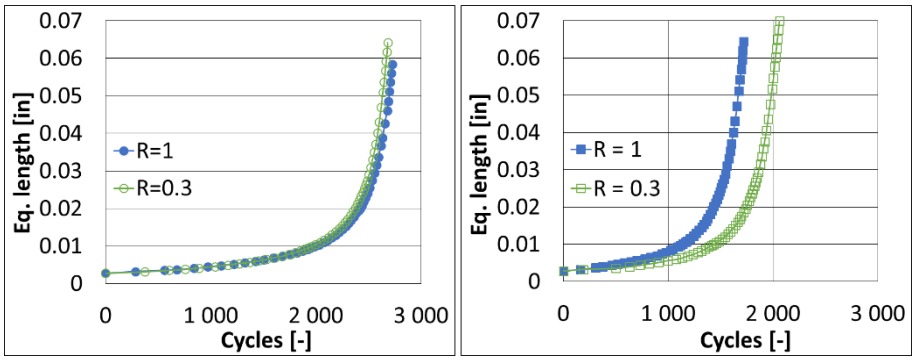


*(a)* *(b)*

***Figure III. 11*** *Comparison on crack sizes vs. cycles plots for small and large submodels and both the methodologies: (a) LC and (b) FD.*

***Table III. 2*** *Runtimes compared for FD and LC approaches.*

| - | DOFs x$10^3$ | Step 0 solving phase [min] |
|---|---|---|
| FD, r = 1 in. | 109 | 773 |
| LC, r = 1 in. | 33 | 22 |
| FD, r = 0.3 in. | 68 | 224 |
| LC, r = 0.3 in. | 14 | 7 |

## *III.7 Remarks*

An enhanced FEM-DBEM submodelling approach, based on the principle of linear superposition to solve fracture problems, has been implemented for a crack-growth simulation in a GE-AVIO aeroengine turbine vane. A benchmark of such enhanced LC approach against a classical FD procedure has been proposed and the advantages in terms of runtimes and accuracy are summarized in the following:

- LC approach is fully automated and permits to predict SIF, then also CGRs and kink angles, with higher accuracy and lower runtimes than for FD approach.
- LC approach allows a remarkable decrease in terms of runtimes for SIF calculations because resorting to pure stress analyses instead of, in this case, thermal-stress analyses (needed for the FD procedure), also needing a less refined mesh to get convergent results.
- LC approach accuracy is enhanced because the boundary conditions on the advancing crack are theoretically "correct" since they are correctly extracted from an uncracked FEM global model, as dictated by the superposition principle. Moreover, this allows also considering continuously updating boundary conditions during the simulation, whereas the FD approach is based on boundary conditions with no update during propagation (even if such update would be theoretically needed).
- LC guarantees a lower sensitivity of results against the distance between the cutting surfaces and crack as proven considering different submodel sizes.
- The fine tuning of crack propagation parameters with the FD procedure is more complex because of two contrasting requirements during a crack-growth simulation: a coarse mesh in order to facilitate the remeshing procedure and, at the same time, a very fine mesh in order to guarantee sufficient accuracy for SIFs calculations.

Future developments of present activity will concern an introduction of more realistic fatigue spectrum, representative of more phases of the turbine engine mission profile (Fig. III.5).

# Chapter IV
# FEM-DBEM application on Wendelstein 7-X structure

## *IV.1 Introduction*

In this paragraph a realistic fatigue life assessment of a structural element of the supporting structure of the machine for the fusion experiment "Wendelstein 7-X" (W7-X) is presented. In particular, several cracks were detected on a Lateral Support Element (LSE) of the W7-X machine and the most critical crack has been here analysed by three distinct FEM-DBEM approaches (§II.2.3): Fixed Displacements (FD), Fixed Loads (FL) and Loaded Crack (LC). Two complex fatigue spectra were adopted to realistically reproduce the operating conditions of the machine. We will show how FD and FL approaches provide an upper and a lower bound for fatigue life predictions, whereas the LC results lye in between such bounds, confirming again that LC approach represents an accurate submodelling strategy by means of which it is possible to solve a generic fracture problem. Further details can be found in the literature (Giannella, 2017a).

## *IV.2 Problem description*

Wendelstein 7-X (W7-X) is the world's largest nuclear fusion experiment of stellarator type (Spitzer, 21958; Xu, 2016) that started operation in 2015 at the Max-Planck-Institute for Plasma-Physics in Greifswald, Germany (Fig. IV.1a; Wolf, 2017). In the machine, a hot helium or hydrogen plasma is confined in a Plasma Vessel (PV) by means of an electromagnetic (EM) field (Fig. IV.1b), reaching a magnitude up to 3 T, provided by 50 non-planar and 20 planar superconducting coils (Fig. IV.1c). In the vacuum created inside the cryostat, the coils are cooled down to a superconducting temperature, close to absolute zero (4 K), using liquid helium. The magnetic cage keeps the 30 cubic metres of ultra-thin plasma suspended inside the PV. Such plasma is heated

up to fusion temperature by microwave heating, allowing for the separation of the electrons from the nuclei of the helium or hydrogen atoms. During the initial operations (Wolf, 2017), helium and subsequently hydrogen plasma were continuously produced in the W7-X with pulse lengths varying from half a second to six seconds and temperatures up to 100 million °C (Klinger, 2017).

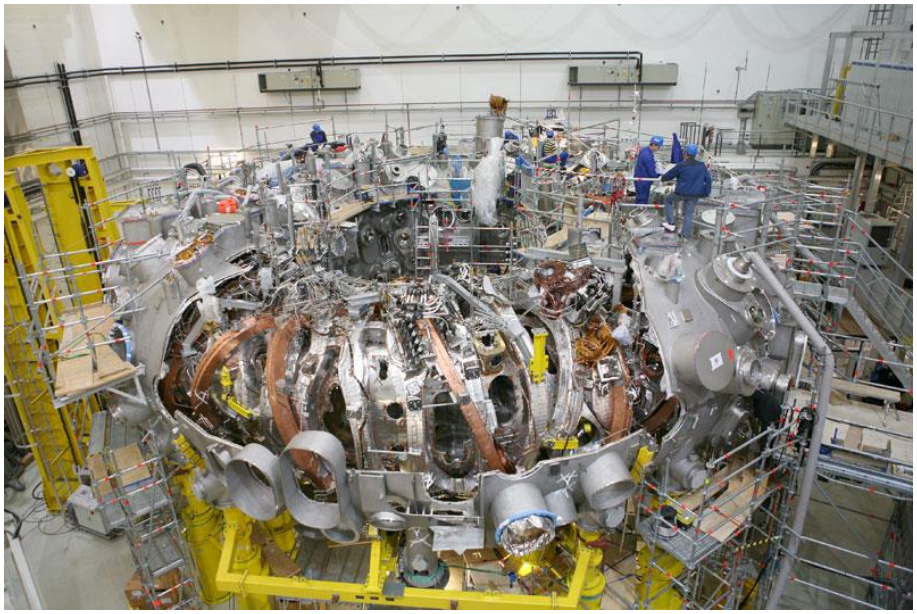

*(a)*

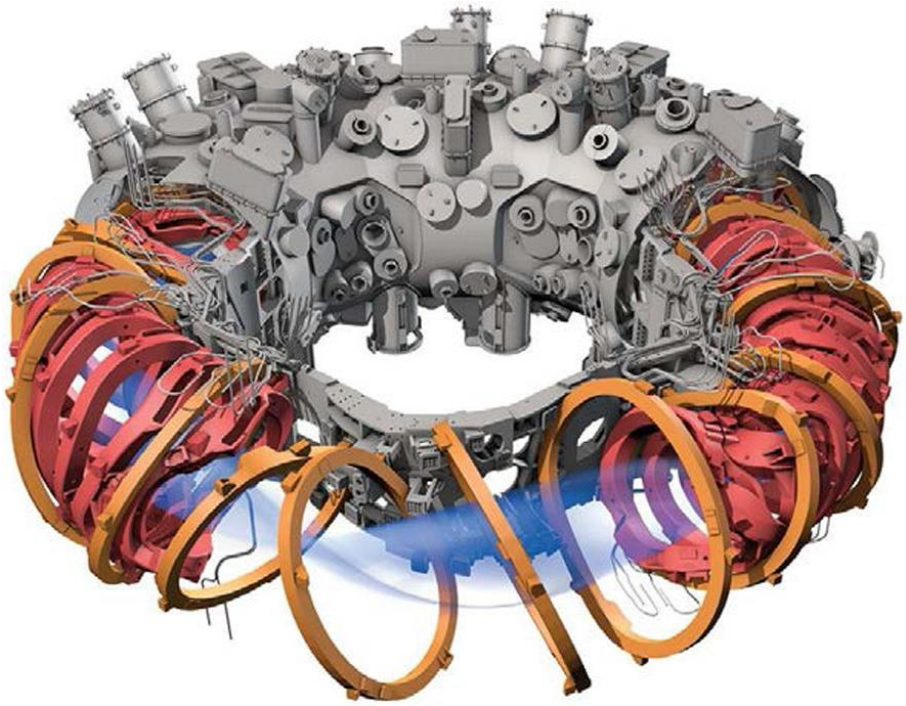

*(b)*

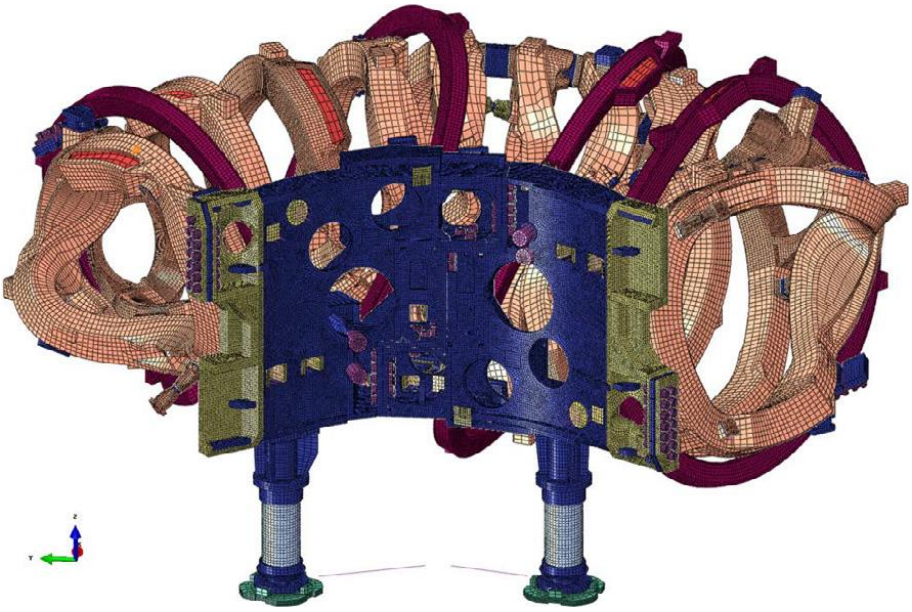

*(c)*

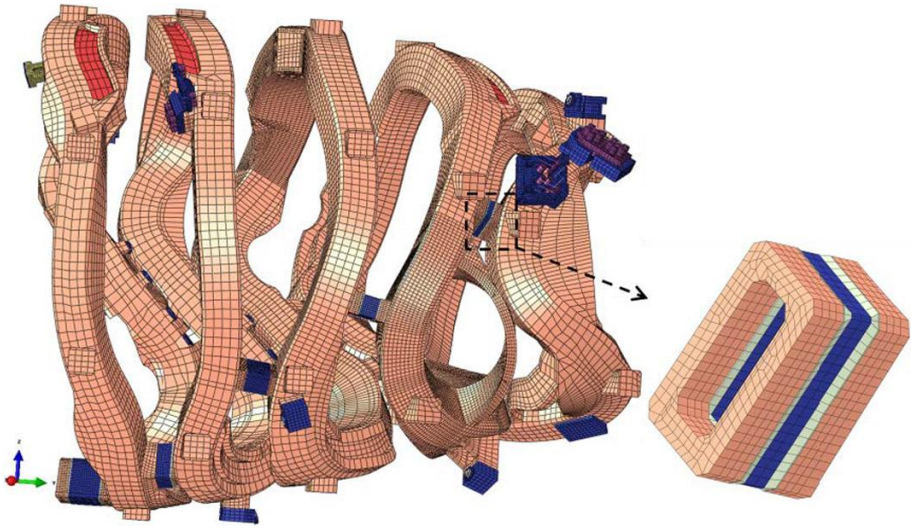

*(d)*

***Figure IV. 1*** *(a) Modular-type stellarator Wendelstein 7-X; (b) Hot plasma confined by EM field generated by the coils; (c) FEM assembly of one-fifth of the magnet system of W7-X; (d) W7-X magnet system: FEM detail of a half module with the LSEs; highlights on the investigated LSE-05.*

The superconducting coils are bolted onto a central support ring and interconnected by welded Lateral Support Elements (LSEs; Fig. IV.1d): 100–150 mm long hollow tubes of 30–35 mm thickness made of forged stainless steel (EN 1.4429).

After the welding of the LSEs to the coil cases (weld depth 15–30 mm), several surface cracks larger than 8 mm (typical acceptance limit of EN 23277, 2010) were found near the welds that could potentially limit the W7-X operations. Cracks were found with visual inspection and dye penetration tests at the accessible surfaces, particularly at the coil side of the weld within the cast steel, oriented mainly parallel to the weld seam (Fig. IV.2). Such cracks, in coils and superconducting cables areas where high stresses develop (Corato, 2015), can become critical during operations.

In order to take advantage of the high accuracy and flexibility of DBEM (Kuranakov, 2016; Alatawi, 2015; Chen, 1999; Hong, 1988) when handling 3D crack-growth under mixed-mode conditions, in (Citarella, 2013) such cracks were modelled using a coupled FEM-DBEM approach (Citarella, 2014, 2016b, 2016c). Crack sizes as well as stress-states and SIFs along the crack front were step-by-step updated through the entire simulation, and the crack-growth was continued until the critical SIF was reached. The crack depth was not pointed out by NDI (Non-Destructive Inspection) tests; however, from repair experience it was found that such size is typically smaller than half the superficial crack length. In (Citarella, 2016c), the same problem was tackled

considering the simultaneous propagation of multiple cracks up to a condition of coalescence.

In this work, the most critical discovered crack (Fig. IV.2) has been modelled with three different FEM-DBEM approaches. The complex global analysis of one fifth of the fivefold W7-X magnet system was worked out with a FEM approach, whereas the fracture problem was tackled by means of a DBEM submodelling strategy. In particular, the adopted approaches are the three loading methods of a generic submodelling problem already presented in §I.3 and shown in Fig. I.3.

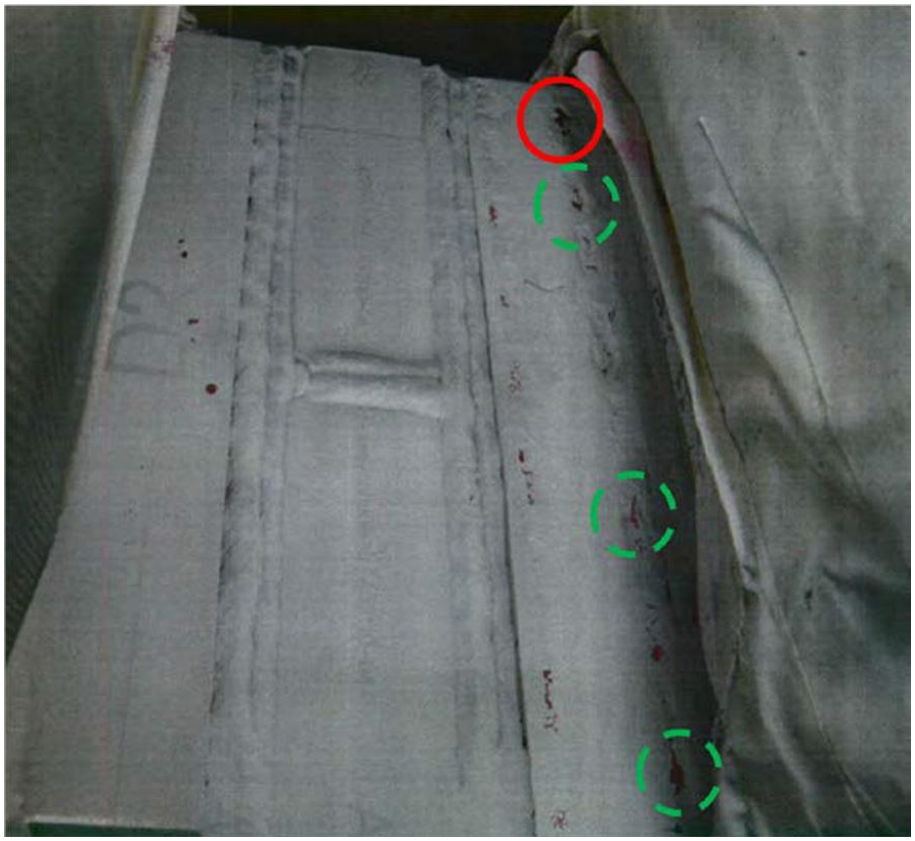

***Figure IV. 2*** *LSE-05: real component with highlight of discovered surface cracks; continuous circle (red line) surrounding the most critical (and modelled) crack.*

The SIF values corresponding to the initial crack configuration are expected to be equal among the FD, FL and LC approaches, whereas differences will start to emerge during the propagation, because boundary conditions are continuously updated along the propagation for LC (as theoretically requested) and are instead kept as "frozen" for FD and FL with consequent introduction of an element of approximation. Moreover, LC life-

prediction is expected to be in between the predictions computed by FD and FL approaches.

The ABAQUS (ABAQUS, 2011) and BEASY (BEASY, 2011) commercial codes are used for FEM and DBEM analyses respectively.

## *IV.3 FEM modelling*

A global FEM model of one fifth of the fivefold symmetric W7-X magnetic cage has been developed (Fig. IV.3a) considering, in addition to the magnetic loads ("HJ" refers to the most critical magnetic field configuration, better explained in §IV.5): bolt preloading, dead weight and cooling. Then, a first FEM submodel (Fig. IV.3b) involving the whole LSE-05 (Fig. IV.3b) has been made (without any crack introduction). In final, a second FEM submodel, involving a smaller part of LSE-05, has been built up (Fig. IV.3c) in order to get a more accurate stress assessment on the cracked area. Namely, with such submodel it has been possible to provide more accurate stress field to load the DBEM crack faces, as requested by the LC approach.

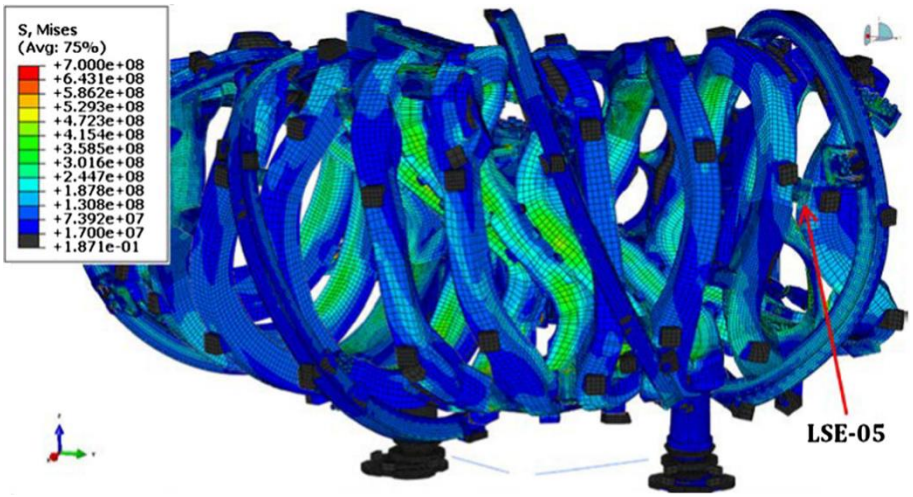


*(a)*

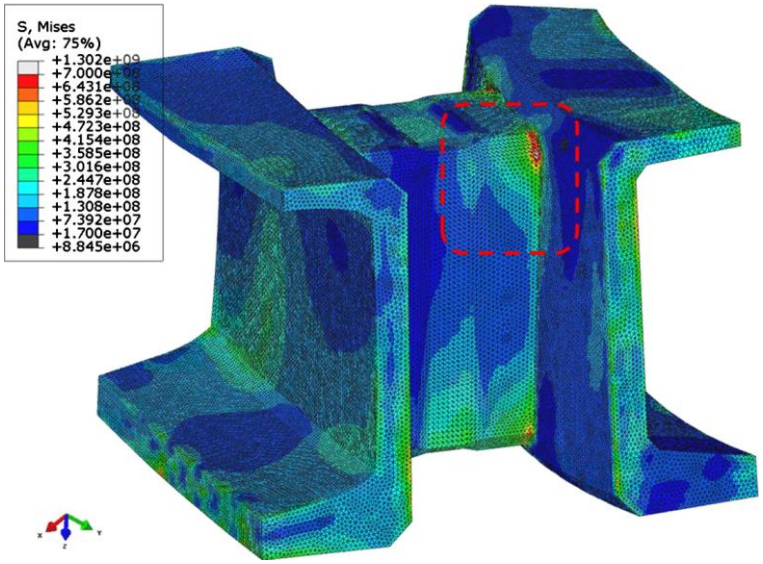


*(b)*

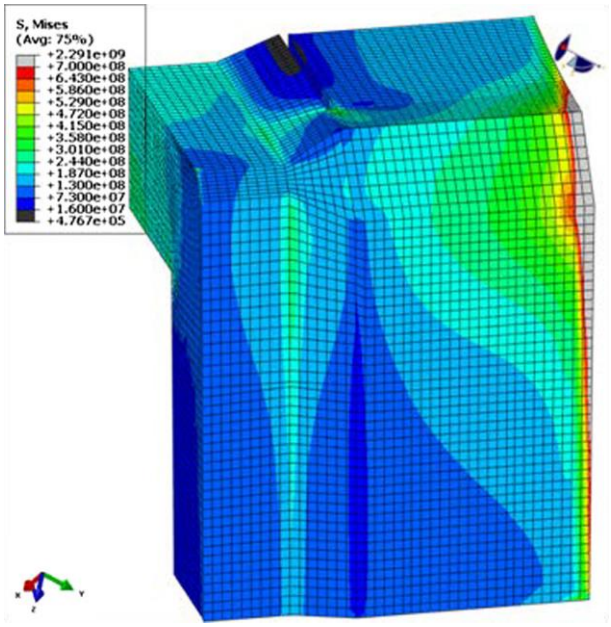


*(c)*

***Figure IV. 3*** *Von Mises stresses [Pa], related to the load case with EM field of 3 T "HJ", on the: (a) FEM global model, (b) first FEM LSE-05 submodel, (c) furtherly reduced FEM submodel. Red arrow in (a) pointing out the submodelled LSE-05 in (b). Dashed red square in (b) representing the area that has been furtherly refined in (c).*

## *IV.4 DBEM modelling*

The DBEM modelling was aimed at simulating the propagation of a semi-circular crack. For this purpose, the crack-growth simulations were performed by using a DBEM cracked submodel, loaded in three different ways as illustrated in §I.3 (Fig. I.3). The crack paths were assessed by resorting to the Minimum Strain Energy Density criterion (§I.4.2; Sih, 1974) and the Stress Intensity Factors (SIFs) along the crack front were calculated by the *J*-integral approach (§I.4.1; Rigby, 1993, 1998).

An uncracked BEM model (Fig. IV.4b) was extracted from the first aforementioned FEM submodel (Fig. IV.3b) by a Boolean operation of subtraction of a spherical domain having the centre on the most critical crack. Then, a semi-circular crack with radius equal to 7 mm was inserted (Fig. IV.5), switching from a BEM to a DBEM formulation, in order to tackle the singularity introduced by the crack modelling.

The spherical domain must be sized in such a way to have a sufficiently large distance between the crack and the cutting surfaces. FD and FL approaches impose this constraint in order to guarantee a sufficient insensitivity of the applied fixed boundary conditions, coming from the uncracked corresponding global model, against the changes introduced by the growing crack. On the other hand, the LC approach generally requests a smaller submodel since it just need to have available a sufficiently large "fading" distance, from the crack to the subdomain boundaries, for the stress field dying out. Nonetheless, the same submodel size has been used in this work for all the three approaches since it satisfied all the different requests. To this aim, a preliminary convergence study was aimed at evaluating such minimum submodel size and the results for this optimal submodel dimension are here presented. As a consequence, the chosen spherical cut has a radius equal to 0.11 m.

The adopted material properties are listed in Tab. IV.1 (see Fig. IV.5 for zone definition). The initial DBEM mesh comprises nearly 5300 elements: the crack faces as well as the crack surroundings are remeshed step-by-step by using quadrilateral 8-node elements and triangular 6-node elements, whereas the non-remeshed areas keep 3 node triangular and 4 node quadrilateral elements for LC and 6 node triangular and 9 node quadrilateral elements for FD/FL. At the last considered propagation step, in correspondence with the biggest crack size, the number of elements rises up to nearly 5800 for all the approaches.

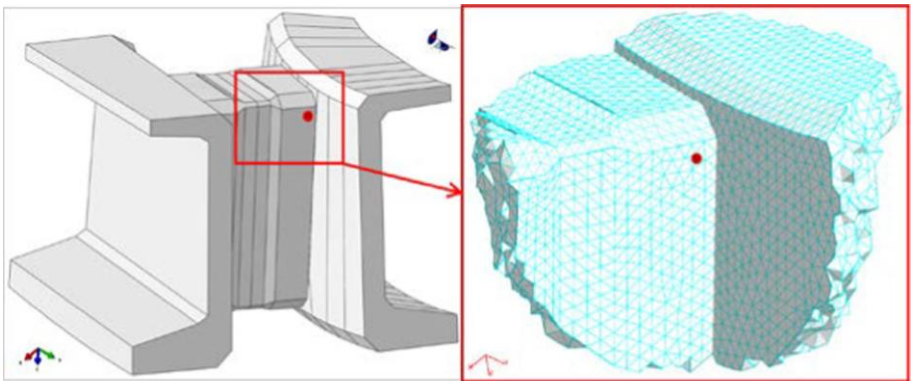

*(a)* *(b)*

***Figure IV. 4*** *(a) FEM submodel and (b) DBEM uncracked submodel (the red dot is the crack insertion point), obtained by a Boolean subtraction with a sphere of radius 0.11 m.*

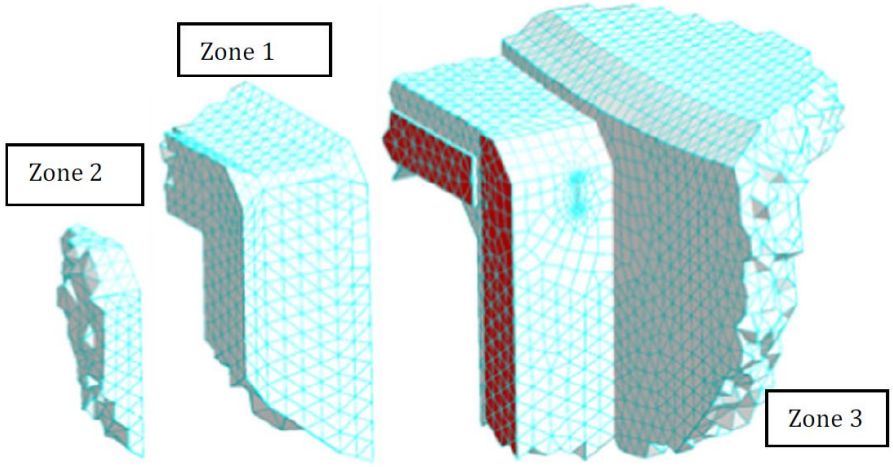


***Figure IV. 5*** *DBEM cracked submodel with highlight of the different modelled zones.*

***Table IV. 1*** *Mechanical properties at temperature of 4 K.*

| Parameter | Zone 1<br>EN 1.4429 | Zone 2, 3<br>EN 1.3960 |
|---|---|---|
| Young's modulus E [GPa] | 197 | 158 |
| Poisson' ratio ν [-] | 0.3 | 0.3 |
| Thermal expansion coefficient α [μm/(mK)] | 10.38 | 10.2 |

As anticipated, different alternatives of boundary conditions were taken into account for the current LEFM problem (Fig. IV.6). Fig. IV.6b represents the DBEM model with LC approach: boundary conditions were only applied on the crack faces and continuously updated along the crack extension. Alternatively, Fig. IV.6a and IV.6c show boundary conditions applied on the DBEM cut surfaces, in terms of either displacements or tractions respectively. In this case, the crack-growth was solved under either FD or FL assumption with no update of BCs during the crack propagation. FD model was already constrained in the three directions whereas some springs of negligible stiffness were added to constrain the model used for FL). Furthermore, BCs for FD/FL are typically computed by a FEM global model that does not contain a crack, then with an inherent approximation whose impact on the results can be restricted only by resorting to a large enough DBEM submodel, in such a way to keep the cut surfaces sufficiently far from crack boundaries. On the other hand, enlarging the submodel will affect the computational burden.

When using the LC approach, an uncracked FEM model is necessary to accurately compute the stress field in the surroundings of the cracked zone, whereas the fracture problem is completely left to the DBEM analysis. All the loads applied to the real component (viz. thermal, electro-magnetic, dead weight, bolt preloading) are incorporated by the FEM analyses, whereas the SIFs evaluation and subsequently the whole crack-growth is worked out into the DBEM environment by means of step-by-step pure stress analyses.

A further advantage of such LC approach is given by the possibility to study crack propagation with a smaller model than that needed by FD/FL approaches, as enabled by the self-equilibrated nature of the load applied with LC and its rapidly vanishing effects when getting slightly far from the crack. Such reduction of the DBEM model size enables a strongly speed up of the calculations.

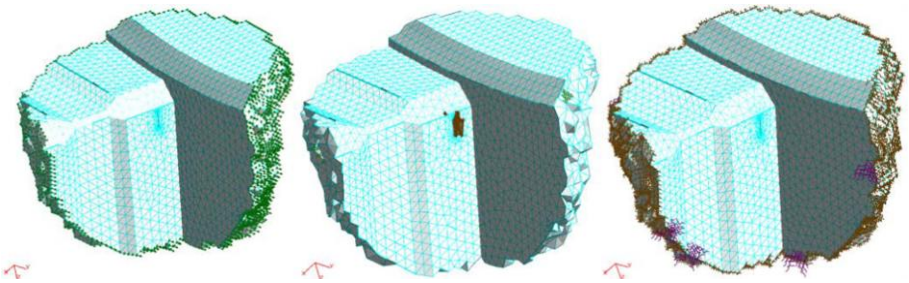

*(a)* *(b)* *(c)*

***Figure IV. 6*** *DBEM submodel loaded with different BCs: either (a) displacements (FD) or (c) tractions (FL) applied on cut surfaces; (b) tractions applied on the crack faces (LC).*

## *IV.5 Fatigue load spectra*

The fatigue load spectra, corresponding to the sequence of five load changes on the magnet, were applied to the DBEM submodel through different boundary condition sets. Such boundary condition sets were obtained from five different FEM global analyses and corresponding FEM submodel analyses. A qualitative visual description of the loading history due to the Lorentz forces is provided in Fig. IV.7.

The FEM analyses were performed using different electromagnetic loadings, so as to build up the following five load cases:

*i.* magnetic field with magnitude equal to 2.5 T with a given orientation (termed "HJ");
*ii.* magnetic field with magnitude equal to 2.5 T with a different orientation (termed "LS");
*iii.* magnetic field with magnitude equal to 3 T in "HJ" configuration;
*iv.* magnetic field with magnitude equal to 3 T in "LS" configuration;
*v.* magnetic field with magnitude equal to 1.7 T in "HJ" configuration. This load corresponds to the reduced magnetic field at night.

Such five load cases were combined for building up two sequences up that corresponded to two fatigue load spectra:

- daily spectrum, using only the load steps from *i* to *iv* (load step *v* was excluded assuming that the magnets are turned off at night); the sequence showed in Tab. IV.2 was repeated up to a condition of crack instability;
- weekly spectrum, using all of the five load cases *i* to *v*; again, the sequence showed in Tab. IV.3 was repeated up to the condition of crack instability.

The plan was that the magnet system remained loaded for a 5-days week of experimental operations, with or without a limited reduction of the electromagnetic (EM) field at nights (Fig. IV.7). During an experimental campaign, the EM field could be shifted several times from one configuration to another ("HJ" to "LS" and vice versa) with changes involving the EM field direction; moreover, there could be also changes to the EM field magnitude, from 2.5 T to 3 T and vice versa.

Consequently, in order to estimate the operational limits of the machine, the following SIF increments were considered:

- $\Delta K_{0-2.5T}$ due to start-up of the machine on Monday morning from 0 to 2.5 T;
- $\Delta K_{2.5T-3T}$ due to increase from 2.5 T to 3 T;
- $\Delta K_{2.5Tij}$ and $\Delta K_{3Tij}$, each one due to shift from one EM configuration to another, considering a magnetic field of and 2.5 or 3 T respectively.

In case of weekly spectrum, $\Delta K_{night}$, related to a moderate reduction of the magnetic field at night, was added. Changes in the EM field for plasma ripple control were considered as small enough to be neglected.

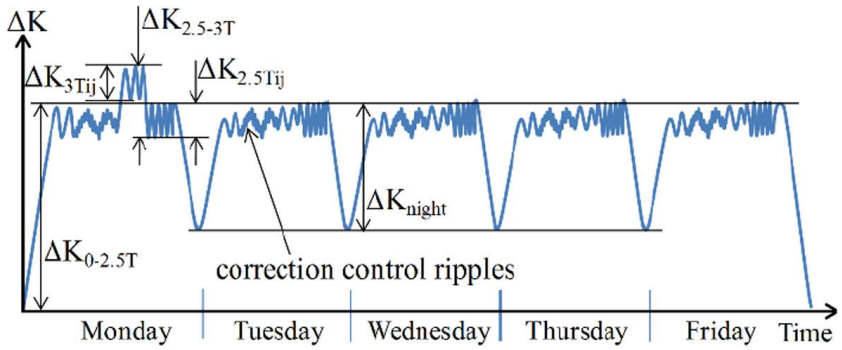


***Figure IV. 7*** *Schematic loading history due to EM forces.*

***Table IV. 2*** *Fatigue elementary block corresponding to 10 working days with the daily spectrum (12.1 cycles per working day).*

| Cycles per block | EM field (minimum magnitude) | EM field (maximum magnitude) |
|---|---|---|
| 10 | 0 | 2.5 T (“HJ” config.) |
| 100 | 2.5 T (“LS” config.) | 2.5 T (“HJ” config.) |
| 1 | 0 | 3 T (“HJ” config.) |
| 10 | 3 T (“LS” config.) | 3 T (“HJ” config.) |

***Table IV. 3*** *Fatigue elementary block corresponding to 50 working days with the weekly spectrum (5.42 cycles per working day).*

| Cycles per block | EM field (minimum magnitude) | EM field (maximum magnitude) |
|---|---|---|
| 10 | 0 | 2.5 T (“HJ” config.) |
| 200 | 2.5 T (“LS” config.) | 2.5 T (“HJ” config.) |
| 1 | 0 | 3 T (“HJ” config.) |
| 20 | 3 T (“LS” config.) | 3 T (“HJ” config.) |
| 40 | 1.7 T (“HJ” config.) | 2.5 T (“HJ” config.) |

The crack-growth for the load cycles from 0 to 2.5 T was predicted by using a Paris’ law (§I.4.3; Paris, 1961):

$$\frac{da}{dN} = C\Delta K^m \tag{I.15}$$

with the related Paris’ parameters listed in Tab. IV.4, as derived from Fatigue Crack-Growth Rate (FCGR) test series carried out at cryogenic

temperatures. On the other hand, the Crack-Growth-Rates (CGRs) for the other cycles related to a stress ratio $R \neq 0$ were predicted using a Forman's law (§I.4.3; Forman, 1967):

$$\frac{da}{dN} = \frac{C\Delta K^m}{(1-R)K_c - \Delta K} \tag{I.16}$$

with the related Forman's parameters listed in Tab. IV.5.

C values are consistent with $\Delta K$ units $[Pa * m^{0.5}]$ and $da$ units $[mm]$.

***Table IV. 4*** *Paris' law parameters at temperature of 4 K.*

| Parameter | Zone 2, 3<br>EN 1.3960 |
|---|---|
| C [-] | 3.314E-32 |
| m [-] | 3.23 |
| $\Delta K_{th}$ $[Pa * m^{0.5}]$ | 15 |
| $K_c$ $[Pa * m^{0.5}]$ | 1.6E8 |

***Table IV. 5*** *Forman's law parameters at temperature of 4 K.*

| Parameter | Zone 2, 3<br>EN 1.3960 |
|---|---|
| C [-] | 1.167E-17 |
| m [-] | 2.36 |
| $\Delta K_{th}$ $[Pa * m^{0.5}]$ | 15 |
| $K_c$ $[Pa * m^{0.5}]$ | 1.6E8 |

## *IV.6 Results*

The boundary conditions of DBEM submodels were provided by the analyses on the FEM submodels for the five different magnetic configurations. Then, the two mentioned fatigue spectra, conforming to the daily and weekly W7-X operating conditions, were built up.

In doing this, three DBEM submodels have been separately loaded applying the boundary condition sets requested by the FD, FL and LC approaches. Regarding the LC, a first attempt of using stresses coming from the FEM submodel shown in Fig. IV.3b did not produce accurate results, so it was necessary to furtherly refine the FEM mesh in the crack surroundings (Fig. IV.3c). This was expected since the accuracy of DBEM results (i.e. SIFs) was completely dependent on the accuracy of stress evaluations on the virtual crack faces provided by the FEM submodel solution.

The crack size definition is shown in Fig. IV.8b; sizes A, C and B were calculated as linear distances between the crack insertion point and the points

on the crack front positioned at a normalised abscissa of 0, 0.5 and 1 respectively.

The DBEM stress field from the LC approach (Fig. IV.9) is not representative of the real stress scenario throughout the whole component that can be instead obtained by FD/FL approaches (Fig. IV.10). Anyway, it is useful to determine accurately SIFs along the crack front (just the crack tip stress singularity can be properly obtained) as dictated by the superposition principle.

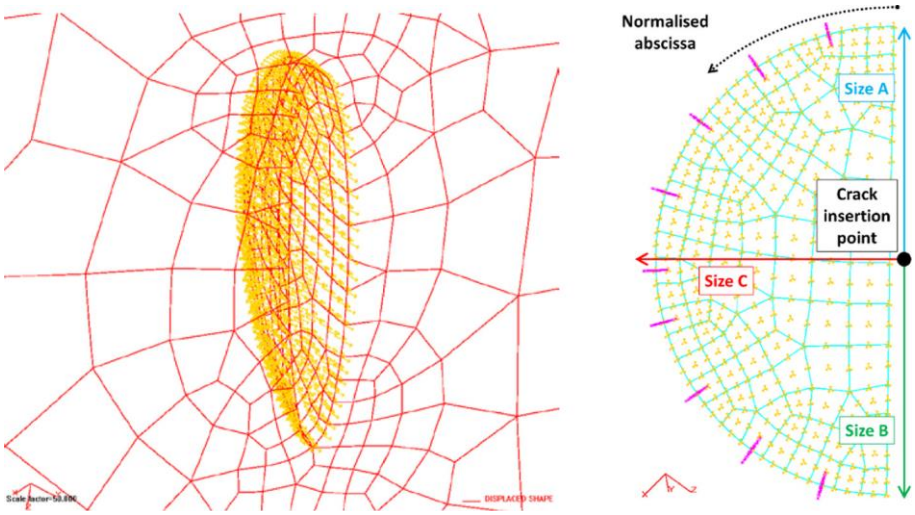


*(a)* *(b)*

***Figure IV. 8*** *(a) DBEM crack (deformed shape) with the applied tractions (in orange) for the LC approach; (b) crack sizes definition with J-paths along crack front (in purple).*

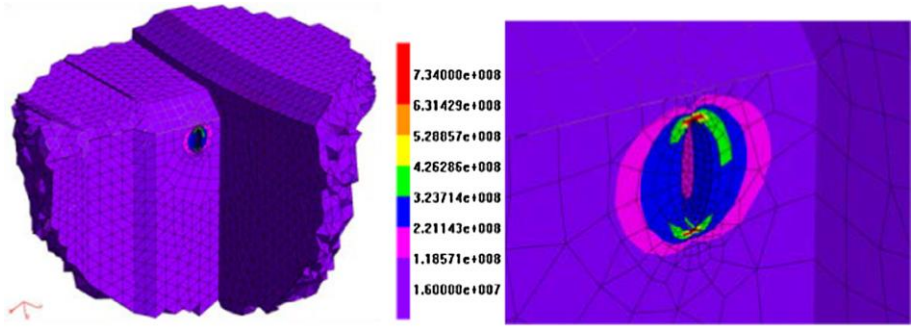


*(a)* *(b)*

***Figure IV. 9*** *(a) Von Mises stress scenario for LC approach; initial crack configuration and load case iii; (b) close up of the von Mises stress scenario in the crack surroundings for LC approach; initial crack configuration and load case iii.*

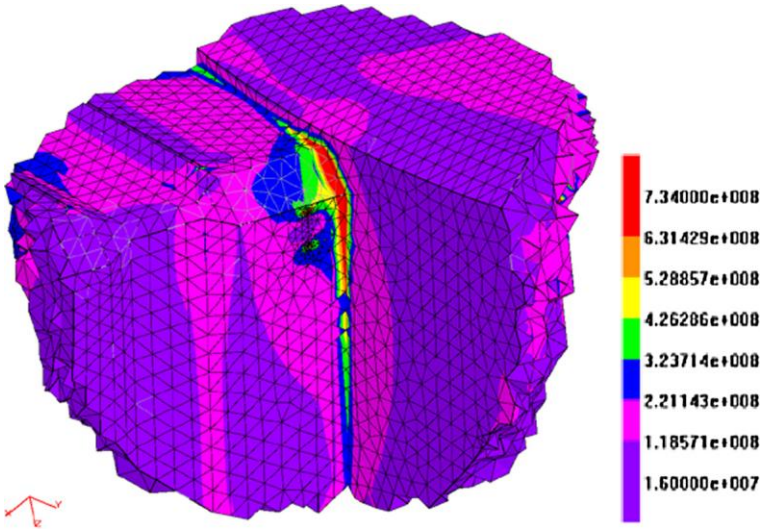


***Figure IV. 10*** *Von Mises stress scenario from FD/FL approach; initial crack configuration and load case iii.*

SIFs computed by the three approaches are compared in Fig. IV.11 for all the five different load cases from *i* to *v*. Such SIFs for the initial crack configuration show a perfect match between the adopted approaches, proving also the correct implementation of the superposition principle to the considered LEFM problem.

Once the FEM analyses were completed and the DBEM submodel created and loaded, step-by-step crack-growths were simulated. Each single growth step was comprehensive of the following phases:

*1)* crack insertion;
*2)* crack faces loading (needed only by the LC approach);
*3)* linear-elastic DBEM analysis and corresponding SIFs evaluation;
*4)* life prediction;
*5)* new crack front prediction.

As previously said, the application of either traction (FL) or displacement (FD) boundary conditions to the DBEM cut surfaces would represent an approximation due to the continuously increasing crack dimensions and the consequential continuously decreasing DBEM model stiffness. In addition, such boundary conditions generally come from a FEM global model in which the presence of the crack is not considered at all. On the contrary, the LC approach does not present such approximations, as the traction boundary conditions applied on the crack faces are rigorously computed from an uncracked FEM domain, as theoretically dictated by the superposition principle. In addition, such crack faces loads are continuously updated through the simulation since further loads are applied on the continuously created crack extensions.

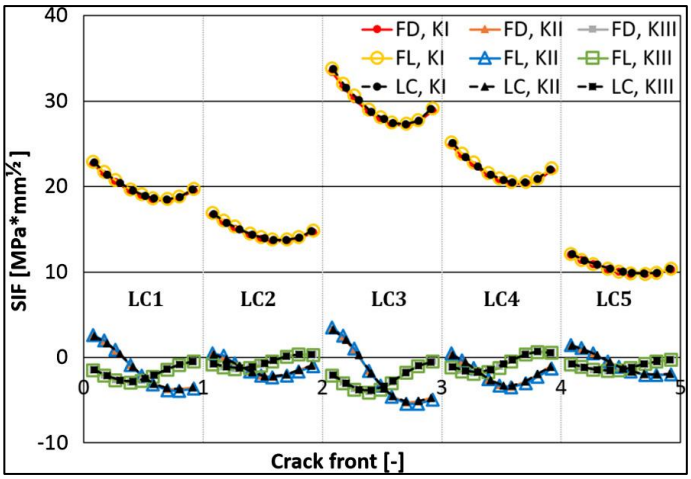


***Figure IV. 11*** *SIF values along the crack front for FD, FL and LC approaches for all the load cases from i to v.*

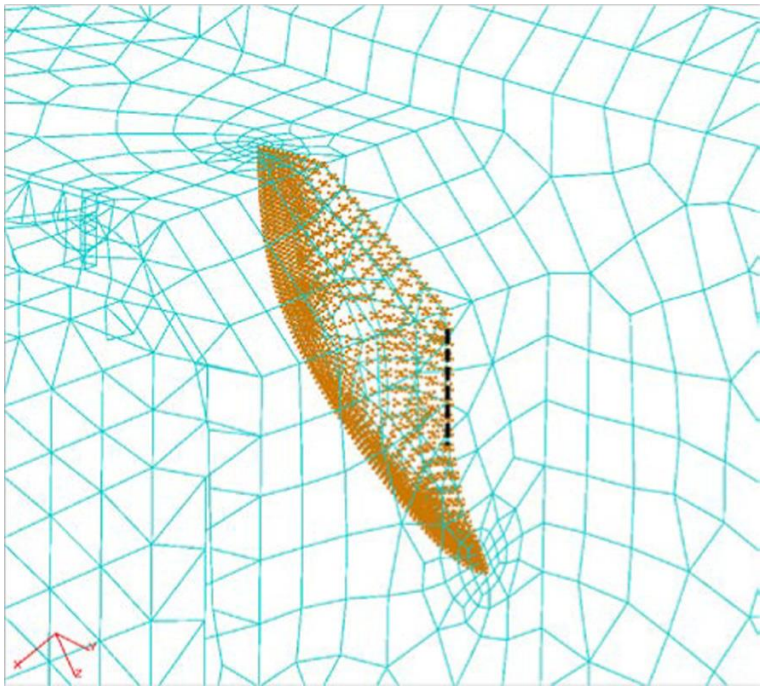

***Figure IV. 12*** *Final crack shape; traction BCs (in orange) applied on the crack face elements for LC approach; dashed black line representing the initial edge of the inserted crack.*

The crack propagations, subdivided in 16 steps, were computed considering an average crack advance per step ranging between 1 mm for the initial steps and 1.5 mm for the last steps. The final considered crack shape,

with the related tractions applied on the crack face elements for LC, is shown in Fig. IV.12: a slight kinking of the growing crack is visible consistently with the slight mixed-mode conditions shown in Fig. IV.11.

Results in terms of crack advance vs. fatigue cycles and $K_{eq}$ during growth for both daily and weekly fatigue spectra are reported in Figs. IV.13 and IV.14 respectively: it is possible to observe that the $K_{eq}$ values, even if higher than threshold, turn out to be lower than $K_c$ up to the final considered scenario, which consequently was judged subcritical.

Equivalent SIF values were computed by using the Yaoming-Mi formula (§I.4.3; Mi, 1995):

$$K_{eq} = \sqrt{(K_I + |K_{III}|)^2 + 2K_{II}^2} \tag{I.19}$$

and its variation in the cycle provided the $\Delta K_{eq}$ to be used in the Paris' and Forman's laws (eqs. I.14 and I.15).

From fig. IV.13, it is possible to observe the progressively increasing difference between the three approaches, dictated by SIF values that are precisely overlapped at the initial step (step 0; Fig. IV.11) and progressively diverging along with the crack extension (Fig. IV.14).

Daily and weekly load spectra appeared to give quite similar fatigue life predictions, as visible from Fig. IV.13, but differences came out if considering on the abscissa the working days rather than the fatigue cycles. As a matter of fact, the daily spectrum predicted a much lower number of working days, before than reaching a critical condition, because the EM field was considered as turned down at night, with consequent less frequent main cycles (those related to the switch-off of the EM field with corresponding strongest variation on SIFs).

In final, a comparison on the runtimes needed by the three different FEM-DBEM approaches is provided in Tab. IV.6. Such runtimes were averaged between analyses with daily and weekly load spectra. LC runtimes were strongly lower than that needed by FD, or equivalently FL. This was due to the smaller DBEM meshes to handle for LC since FD/FL required finer meshes to get convergent results.

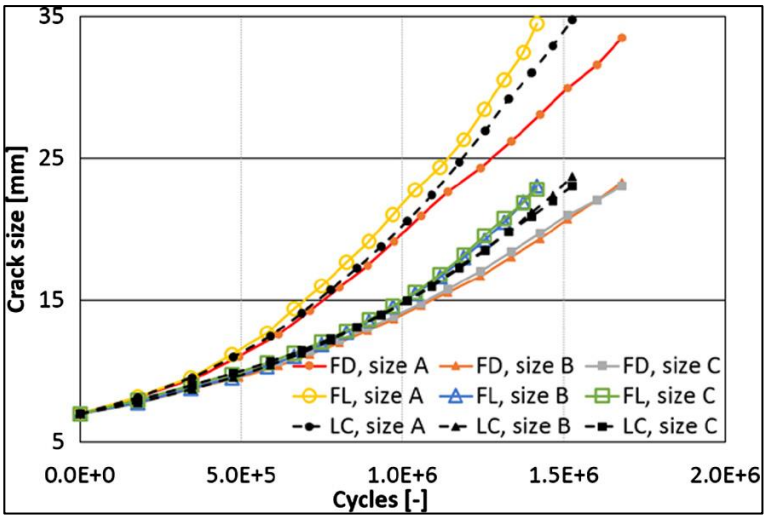


*(a)*

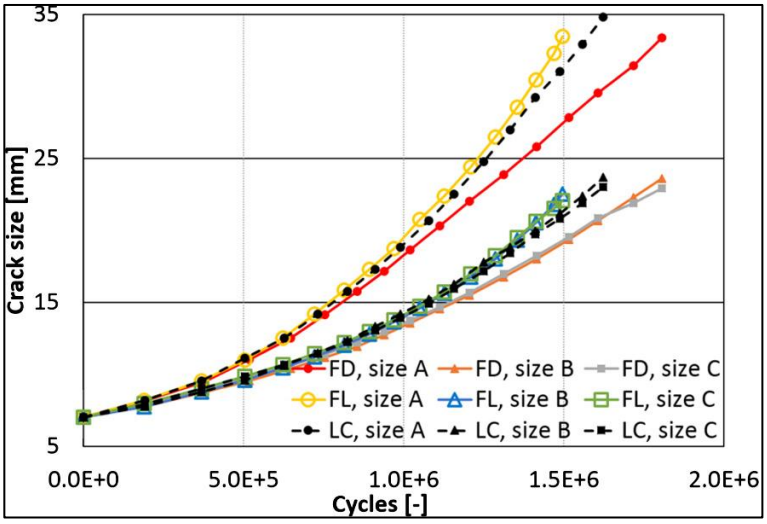


*(b)*

***Figure IV. 13*** *Crack sizes vs. number of cycles under (a) daily and (b) weekly load spectra.*

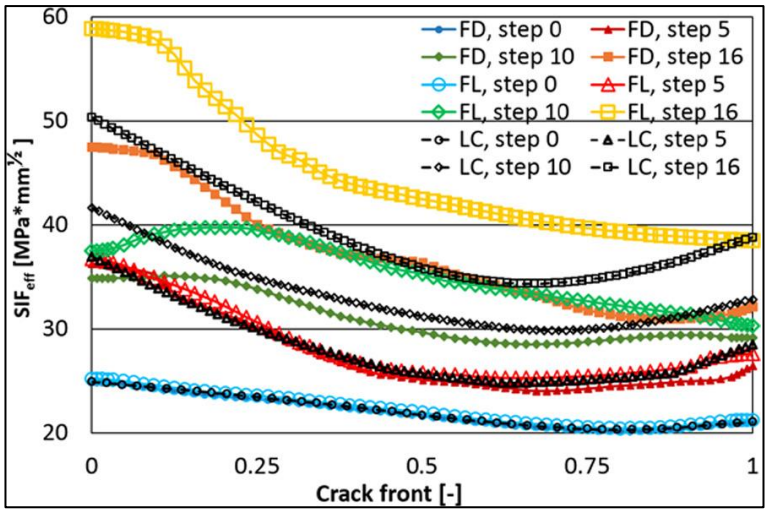


*(a)*

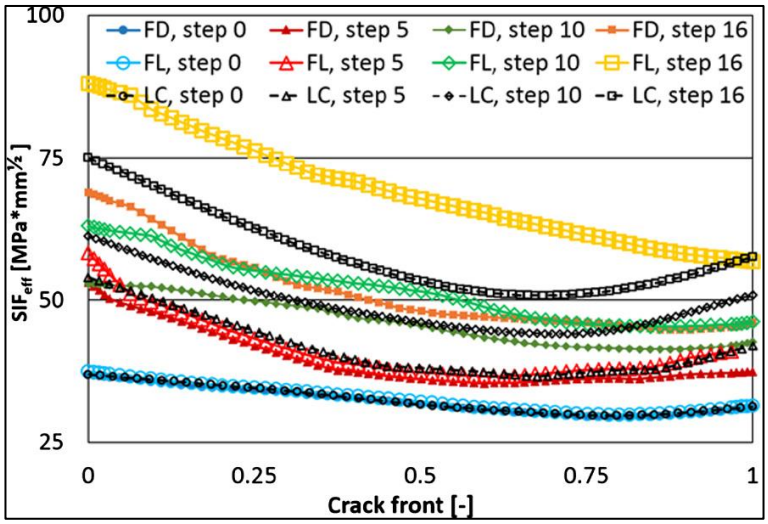


*(b)*

***Figure IV. 14*** *Equivalent SIFs vs. number of cycles under (a) daily and (b) weekly load spectra.*

***Table IV. 6*** *Runtimes comparison between FD/FL and LC.*

| DBEM analyses | FD/FL | LC | FD/FL – LC comparison |
|---|---|---|---|
| SIFs at initial step | 59 | 21 | -64% |
| SIFs at final step | 151 | 27 | -82% |
| Whole crack-growth | 1704 | 414 | -76% |

## *IV.7 Remarks*

Crack-growth simulations have been performed to analyse the behaviour of the most critical crack detected on the Wendelstein 7-X Lateral Support Element 05. The simulations have been performed realistically considering the machine operations by means of the adoption of two different fatigue load spectra: weekly and daily operating conditions.

The proposed approach leverages on a submodelling technique to strongly reduce the computational efforts. Moreover, such submodelling has been put in place by using the coupling of FEM and DBEM methods in three different ways: two "classical" "Fixed Displacements" and "Fixed Loads" approaches have been compared with an enhanced "Loaded Crack" approach. Such LC approach, in which the DBEM loads consist of just tractions calculated in the global FEM analysis and applied on the DBEM crack face elements, allowed to work out the LEFM problem with some advantages over the FD or FL approaches, in terms of accuracy and runtimes.

Although SIF values along crack front provided by the FD, FL and LC were perfectly overlapped for the initial crack configuration, differences arisen when the crack grew through the DBEM domain. The reason was twofold: the FD/FL methods did not consider the variability of BCs along with the crack-growth and suffer from an approximation when using a FEM uncracked model to obtain the DBEM boundary conditions. On the contrary, the LC approach, updating step-by-step the BCs with which it computes SIFs, circumvents the approximations above described, predicting CGRs whose values lies in between those provided by the conservative FL and non-conservative FD approaches.

Several advantages of LC, in terms of accuracy as well as runtimes, against the classical approaches with fixed displacement/traction boundary conditions, have been presented and discussed in this work.

This work turned out to be a very useful example of how it is possible to judge the risk of unstable crack-growth when considering very large and complex structures.

# Conclusions

The thesis presented a smart submodelling procedure to numerically simulate general Linear Elastic Fracture Mechanics (LEFM) problems.

Such procedure leverages on the implementation of the principle of linear superposition to submodelling for Fracture Mechanics (FM) problems. Fundamentally, with the proposed procedure, the crack tip stress singularity can be properly captured without considering any external load but just load applied on the crack faces, evaluated from the original global problem without the crack insertion (the latter will be only introduced in the submodel).

The numerical procedure exploits simultaneously the different advantages of the Finite Element Method (FEM) and the Dual Boundary Element Method (DBEM), with the aim to achieve very accurate assessments of the LEFM parameters, i.e. Stress Intensity Factors (SIFs) along the crack fronts, deflection angles of the cracks, Crack Growth Rates (CGRs), etc.

When facing fracture problems, it is often needed to resort to submodelling techniques to strongly reduce the computational burden, especially when dealing with very large engineering structures.

The procedure presented in this thesis is based on a smart submodelling strategy in which the FEM is used to work out the non-damaged problem while the DBEM is used for the fracture assessment on a submodel extracted from the global domain. This allows profiting by both the wide versatility of FEM together with the high potentials of DBEM to manage the fracture aspects.

The thesis presented some theoretical background about the BEM and DBEM and well-established criteria for predicting various FM parameters. Then, some applications of the proposed FEM-DBEM "Loaded Crack" (LC) approach have been presented and compared with experimental results and with numerical results provided by different fracture codes and alternative submodelling approaches, such as "Fixed Displacements" (FD) and "Fixed Loads" (FL).

LC approach demonstrated to be the most accurate submodelling strategy among all the considered approaches, allowing circumventing all the approximations unavoidably introduced by FD/FL. Moreover, LC approach, as implemented through DBEM, turned out to be more efficient then FEM

implementations, since the adoption of DBEM allowed bypassing well-known problems of finite elements when tackling three-dimensional complex shaped cracks (like distortion, huge meshes, etc.). Finally, LC approach demonstrated to be also the most efficient in terms of runtimes for all the benchmarks presented in this work.

The presented LC submodelling procedure can then be adopted as an effective tool for very accurate fracture assessments, becoming very attractive especially when dealing with complex industrial applications, thanks to the fact that it only needs as inputs FEM results of uncracked problems, easily retrievable in the industrial CAE engineering departments.

# References


Alatawi, I. A. and Trevelyan, J. (2015) A direct evaluation of stress intensity factors using the Extended Dual Boundary Element Method. *Eng Anal Boundary Elements*, **52**, 56–63.

Aliabadi, M. H. (1990) Evaluation of mixed mode stress intensity factors using path independent integral, *Proc. 12th Int. Conf. on Bound. Element Methods*, Computational Mechanics Publications, Southampton, 281-292.

Aliabadi, M. H. and Rooke, D.P. (1992a) Numerical Fracture Mechanics. *Computational Mechanics Publications Southampton*, Boston.

Aliabadi, M. H. and Brebbia, C. A. (1992b) Advances in Boundary Element Methods for Fracture Mechanics. *Computational Mechanics Publications*, Boston.

Aliabadi, M. H. (2002) The Boundary Element Method, Volume 2, Applications in Solids and Structures, *John Wiley and Sons*, England.

Anderson, T. L. (1991) Fracture Mechanics fundamentals and applications. *Department of Mechanical Engineering*, Texas A&M University.

Apicella, A., Citarella, R., Esposito, R. (1994). Sulla previsione della propagazione per fatica di cricche multiple tramite elementi di contorno discontinui, Proc. of *XXIII CONVEGNO NAZIONALE AIAS*, Rende, 1994.

BEASY V10r14 (2011) Documentation. C.M. BEASY Ltd.

Berto, F., Cendón, D. A., Lazzarin, P. and Elices, M. (2013) Fracture behaviour of notched round bars made of PMMA subjected to torsion at −60°C. *Eng Fract Mech.,* **102**, 271- 287.

Betti, E., (1872) Teoria dell'elasticità, *Il Nuovo Cimento*, 7-10.

Brebbia, C. A. and Dominguez, J. (1977) Boundary Element Method for Potential Problems. *Appl. Math. Modelling*, **1**, 372-378.

Brebbia, C. A. (1978) Weighted Residual Classification of Approximate Methods. *Appl. Math. Modelling*, **2**, 160-164.

Brebbia, C. A., Telles, J. C. F. and Wrobel, L. C. (1984) Boundary Element Techniques. *Springer Verlag*, Berlin.

Brebbia, C. A. and Dominguez, J. (1989) Boundary Elements- "An Introductory Course". *Computational Mechanics Publications*, Southampton, U.K.

Bremberg, D. and Dhondt, G. (2008) Automatic crack- insertion for arbitrary crack growth. Eng Fract Mech., **75**, 404- 416.

Bremberg, D. and Dhondt, G. (2009) Automatic 3- D crack propagation calculations:a pure hexahedral element approach versus a combined element approach. *Int J Fract.*, **157**, 109- 118.

Carlone, P., Citarella, R., Lepore, M. and Palazzo, G. S. (2015) A FEM-DBEM investigation of the influence of process parameters on crack growth in aluminium friction stir welded butt joints. *Int. J. Mater. Form.*, **8**(4), 591–599.

Chen, J. T. and Hong, H. -K. (1999) Review of dual boundary element methods with emphasis on hypersingular integrals and divergent series. *Appl Mech Rev*, ASME, **52**(1), 17–33.

Citarella, R. and Cricrì, G. (2010) Comparison of DBEM and FEM Crack Path Predictions in a notched Shaft under Torsion. *Engineering Fracture Mechanics*, **77**, 1730-1749.

Citarella, R., Lepore, M., Fellinger, J., Bykov, V. and Schauer, F. (2013) Coupled FEM-DBEM method to assess crack growth in magnet system of Wendelstein 7-X, *Frattura ed Integrità Strutturale*, **26,** 92-103.

Citarella, R., Cricrì, G., Lepore, M., Perrella, M. (2014) Thermo-mechanical crack propagation in aircraft engine vane by coupled FEM–DBEM approach. *Advances in Engineering Software*, **67**, 57-69.

Citarella, R., Giannella, V. and Lepore, M. (2015a) DBEM crack propagation for nonlinear fracture problems. *Frattura ed Integrità Strutturale*, **9**(34), 514-523.

Citarella, R., Lepore, M., Maligno, A. and Shlyannikov, V. (2015b) FEM simulation of a crack propagation in a round bar under combined tension and torsion fatigue loading. *Frattura e Integrità Strutturale*, **31**, 138- 147.

Citarella, R., Carlone, P., Lepore, M. and Sepe, R. (2016a) Hybrid technique to assess the fatigue performance of multiple cracked FSW joints. *Engng Fract Mech*, **162**, 38–50.

Citarella, R., Giannella, V., Vivo, E. and Mazzeo, M. (2016b) FEM-DBEM approach for crack propagation in a low pressure aeroengine turbine vane segment. *Theor Appl Fract Mech*, **86**, 143–52.

Citarella, R., Lepore, M., Perrella, M. and Fellinger, J. (2016c) Coupled FEM-DBEM approach on multiple crack growth in cryogenic magnet system of nuclear fusion experiment 'Wendelstein 7-X'. *Fatigue Fract Eng Mater Struct*, **39**, 1488–502.

Citarella, R., Giannella, V., Lepore, M. and Dhondt, G. (2018) Dual boundary element method and finite element method for mixed- mode crack propagation simulations in a cracked hollow shaft. *Fatigue Fract Eng Mater Struct*, **41**(1), 84-98.

Corato, V. et al. (2015) Detailed design of the large-bore 8T superconducting magnet for the NAFASSY test facility. *Supercond Sci Technol.*, **28**, 1–9.

Cruse, T. A. (1969) Numerical solutions in three-dimensional elastostatics. *International Journal of Solids and Structures*, **5**, 1259-1274.
Dassault Systems Simulia Corp (2011) *Abaqus analysis user's manual*, Version 6.12.1. Providence, RI, USA.
dell'Erba, D. H. and Aliabadi, M. H. (2000) On the solution of three-dimensional thermoelastic mixed-mode edge crack problems by the dual boundary element method. *Engineering Fracture Mechanics*, **66**, 269-285.
Dhondt, G., Chergui, A. and Buchholz., F. - G. (2001) Computational fracture analysis of different specimens regarding 3D and mode coupling effects. *Eng Frac Mech.*, **68,** 383- 401.
Dhondt, G. (2014) Application of the Finite Element Method to mixed-mode cyclic crack propagation calculations in specimens. *International Journal of Fatigue*, **58**, 2–11.
Dhondt, G., Rupp, M. and Hackenberg, H. –P. (2015) A modified cyclic crack propagation description. Engineering Fracture Mechanics, **146**, 21-30.
Dhondt, G. and Wittig, K. (2016) www.calculix.de.
EN ISO 23277. CEN, Brussels; 2010.
Erdogan, F., Sih, G. C. (1963) On the extension of plates under plane loading and transverse shear. *J Basic Engng*, **85D**(4), 519–27.
Fedelinsky, P., Aliabadi, M. H. and Rooke, D. P. (1994) The Dual Boundary Element Method for Dynamic Analysis of Cracked Pin-Loaded Lugs. *Transactions on Engineering Sciences*, **6**, 571-578.
Forman, R. G., Kearney, V. E. and Engle, R. M. (1967) Numerical analysis of crack propagation in cyclic-loaded structures. *J Basic Eng Trans*, ASME **89**, 459–64.
Forman, R. G.; Shivakumar, V. and Newman, J.C. (1993) Fatigue Crack Growth Computer Program "NASA/FLAGRO" Version 2.0" *National Aeronautics and Space Administration Lyndon B. Johson Space Center*, Houston, Texas.
Fredholm, I., (1903) Sur une class d'equations fonctionsless, *Acta Mathematica*, **27**, 365-390.
Giannella, V., Fellinger, J., Perrella, M. and Citarella, R. (2017a) Fatigue life assessment in lateral support element of a magnet for nuclear fusion experiment "Wendelstein 7-X". *Engineering Fracture Mechanics*, **178**, 243-257.
Giannella, V., Perrella, M. and Citarella, R. (2017b) Efficient FEM-DBEM coupled approach for crack propagation simulations. *Theoretical and Applied Fracture Mechanics*, **91**, 76-85.
Green, G., (1828) An Essay on the Application of Mathematical Analysis to the Theories of Electricity and Magnetism, Nottingham, England: T. Wheelhouse.
Griffith, A. A. (1921) The Phenomena of Rupture and Flow in Solids. *Phil. Trans. R. Soc.* A, **221**, 163-198.

Griffith, A. A. The Theory of Rupture. Proc. of the *1st Int. Congr. Appl. Mech.*, 1924, Delft, p.55-63.

Hong, H. –K. and Chen, J. T. (1988) Derivations of integral equations of elasticity. *J Eng Mech*, ASCE, **114**(6), 1028-1044.

https://en.wikipedia.org/wiki/Turbine_engine_failure#/media/File:Delta_Airlines_Flight_1288_Engine_Failure.jpg

Huber, O., Nickel, J. and Kuhn, G. (1993) On the decomposition of the *J*-integral for 3D crack problems. *International Journal of Fracture*, **64**, 339-348.

Ishikawa, H., Kitagawa, H. and Okamura, H., (1980) J-integral of a mixed-mode crack and its application. *Proc. 3rd Int. Conf. on Mechanical Behaviour of Materials*, Pergamon Press, Oxford, vol3, 447-455.

Klinger, T. (2017) Performance and properties of the first plasmas of Wendelstein 7-X. *Plasma Phys Control Fusion*, **59**, 014018.

Kupradze, V. D., (1965) Potential Methods in the Thoery of Elasticity, *Israel Programme for Scientific Translations*, Jerusalem.

Kuranakov, D. S., Esipov, D. V., Lapin, V. N. and Cherny, S. G. (2016) Modification of the boundary element method for computation of three-dimensional fields of strain–stress state of cavities with cracks. *Eng Fract Mech.*, **153**, 302–18.

Lachat, J. C. (1975) A further development of the boundary integral technique for elastostatics. PhD thesis, *University of Southampton*.

Lachat, J. C. and Watson, J. O. (1976) Effective numerical treatment of boundary integral equations: A formulation for three-dimensional elastostatics, *International Journal for Numerical Methods in Engineering*, **10**, 991-1005.

Marcon, M., Cendón, D. A., Berto, F., Lazzarin, P. and Elices, M. (2014) Fracture behavior of notched round bars made of gray cast iron subjected to torsion. *Key Eng Mater.*, **627,** 69- 72.

McNamee, M. J., Leung, K. L. and Zeverech, P. B. Coupling of MSC/NASTRAN and BEM Structural Matricies. *United Technologies Corporation USBI Co.*, Huntsville, Alabama, 35807, U.S.A.

Mi, Y. and Aliabadi, M. H. (1994) "Three-dimensional crack growth simulation using BEM. *Computers & Structures*, **52**(5), 871-878.

Mi, Y. (1995) Three dimensional dual boundary element analysis of crack growth. Ph.D. Thesis. *University of Portsmouth*, USA.

Mikhlin, S. G., (1957) Integral Equations, *Pergamon Press*, London.

NASGRO® Fracture Mechanics and Fatigue Crack Growth Analysis Software. Version 4.02, *NASA-JSC and SwRI*, September 2002.

Paris, P., Gomez, M. and Anderson, W. (1961) A rational analytic theory of fatigue. *Trends Eng*, **13**, 9–14.

Paris, P. C. (1962) The Crack Growth of Fatigue Cracks Due to Variation in Load. PhD. Thesis, *Lehigh University*, Bethlehen.

Parker, E. R. (1957) Brittle Behavior of Engineering Structures. National Academy of Sciences, National Research Council, *John Wiley & Sons*, New York.
Portela, A., (1990) Dual Boundary Element Analysis of Crack Growth. In: Topics in Engineering, Volume 14, *Computational Mechanics Publications*, Southampton UK.
Portela, A., Aliabadi, M. H. and Rooke, D. P. (1993) Dual Boundary Incremental Analysis of Crack Propagation. *Int Journal Computers and Structures*. **46**, 237-247.
Rigby, R. H. and Aliabadi, M. H. (1993) Mixed-mode J-integral method for analysis of 3D fracture problems using BEM. *Eng. Anal. Boundary Elem.*, **11**, 239–256.
Rigby, R. H. and Aliabadi, M. H. (1998) Decomposition of the mixed-mode J-integral – revisited. *Int. J. Solids Struct.*, **35**(17), 2073–2099.
Rizzo, F. J. (1967) An integral equation approach to boundary value problems of classical elastostatics. *Quarterly Journal of Applied Mathematics*, **25**, 83-95.
Sih, G. C. (1974) Strain energy density factor applied to mixed mode crack problems. *Int J Fract.*, **10**, 305- 321.
Somigliana, C., (1886) Sopra l'equilibrio di un corpo elastic isotrope, *Il Nuovo Cimento, serie III*, **20**, 181-185.
Spitzer, L. (1958) The stellarator concept. *Phys. Fluids*, **1**, 253.
Tanaka, K. (1974) Fatigue crack propagation from a crack inclined to the cyclic tensile axis. *Engineering Fracture Mechanics*, **6**, 493-500.
Walker, K. (1970) The Effect of Stress Ratio During Crack Propagation and Fatigue for 2024-T3 and 7075-T6 Aluminum. *American Society for Testing and Materials*, ASTM STP 462.
Wilson, W, K. and Yu, I. -W. (1979) The use of the J-integral in thermal stress crack problems. *Int. J. Fract.*, **15**, 377–387.
Wolf, R. C., Giannella, V. t al. (2017) Major results from the first plasma campaign of the Wendelstein 7-X stellarator. *Nucl. Fusion*, **57**(10), 102020.
Xu, Y. (2016) A general comparison between tokamak and stellarator plasmas. Matter and Radiation at Extremes, **1**(4), 192-200.
Zencrack 7.9- 3 (2015) *Zentech International Limited*, UK.

# Nomenclature

| | |
|---|---|
| K | Stress Intensity Factor (SIF) |
| $K_I$ | Mode I Stress Intensity Factor |
| $K_{II}$ | Mode II Stress Intensity Factor |
| $K_{III}$ | Mode III Stress Intensity Factor |
| $K_{min}$ | Minimum value of Stress Intensity Factor |
| $K_{max}$ | Maximum value of Stress Intensity Factor |
| $K_c$ | Critical value of Stress Intensity Factor |
| $K_{th}$ | Threshold value of Stress Intensity Factor |
| $K_{eq}$ | Equivalent value of Stress Intensity Factor |
| $J$ | J-integral |
| $\Gamma_\rho$ | Closed path enclosing the crack tip |
| W | Strain energy |
| $\omega$ | Path defined by the crack faces |
| $\sigma_{ij}$ | Total stress tensor |
| $\sigma_0$ | Precracking stress field |
| $\overline{J^I}$ | Mode I J-integral |
| $J^{II}$ | Mode II J-integral |
| $J^{III}$ | Mode III J-integral |
| $J^S$ | J-integral symmetric part |
| $J^{AS}$ | J-integral anti-symmetric part |
| $E$ | Young's modulus |
| $\nu$ | Poisson's ratio |
| $\mu$ | Shear modulus |
| $S(\theta)$ | Strain energy density |
| $r$ | Cylindrical coordinate N°1 at crack tip |
| $\theta$ | Cylindrical coordinate N°2 at crack tip |
| $\varphi$ | Cylindrical coordinate N°3 at crack tip |
| $a_{ij}$ | MSED parameter ij |
| $S_{min}$ | Minimum value of strain energy density |
| $S_{cr}$ | Critical value of strain energy density |
| $da/dN$ | Crack-Growth Rate (CGR) |
| $\Delta K$ | Range of Stress Intensity Factor |

| | |
|---|---|
| $C$ | Crack-growth law coefficient |
| $m$ | Crack-growth law exponent |
| $R$ | Stress ratio |
| $w$ | Walker law parameter |
| $f$ | NASGRO law parameter N° 1 |
| $p$ | NASGRO law parameter N° 2 |
| $q$ | NASGRO law parameter N° 3 |
| $f_s$ | Static friction coefficient |
| $\delta$ | Shaft/hub interface clearance |
| $a$ | Crack dimension N° 1 |
| $c$ | Crack dimension N° 2 |
| $G_{eff}$ | Effective value of energy release rate |
| α | ZENCRACK parameter N° 1 |
| $B$ | ZENCRACK parameter N° 2 |
| $r$ | DBEM cut sphere radius |
| cfes | Crack front element size |
| DOFs | Degrees of freedom |
| α | Thermal expansion coefficient |